ISSN 0915-633X

NATIONAL INSTITUTE FOR FUSION SCIENCE

Bifurcations from Periodic Solution in a Simplified Model of Two-dimensional Magnetoconvection

N. Bekki and T. Karakisawa

(Received - Dec. 20, 1994)

NIFS-332 Jan. 1995

RESEARCH REPORT
NIFS Series

NAGOYA, JAPAN

Bifurcations from periodic solution in a simplified model of two-dimensional magnetoconvection

N. Bekki and T. Karakisawa

College of Engineering, Nihon University
Koriyama, Fukushima 963, Japan

December 8, 1994

Abstract

We study a two-dimensional Boussinesq fluid with the nonlinear interaction between the Rayleigh-Bénard convection and an externally imposed magnetic field. We introduce a simplified model of fifth-order system of nonlinear ordinary differential equations with five parameters and integrate it numerically in some parameter regions. We find various types of bifurcations from periodic solutions : period-doubling bifurcation, heteroclinic bifurcation, intermittency and abnormal transition to chaos. We also derive a normal form equation from our fifth-order system, applying the center manifold theory to it, and give an expression for the renormalized Holmes-Melnikov boundary to evaluate numerical results. By means of the normal form equation, we show that each property of the two phase portraits described by the Duffing equation and the van der Pol equation emanates from one common attractor in the five-dimensional space of the fifth-order system.

Keywords: Boussinesq fluid, Rayleigh-Bénard convection , Bifurcation, Period-doubling, Heteroclinic, Intermittency, Chaos, Holmes-Melnikov boundary

1 Introduction

A numerical analysis based on numerical computations may explode a part of the difficulties of nonlinearity in physics. In the past about 30 years there have been two explosions in nonlinear physics. One explosion is that Zabusky and Kruskal[1] found a concept of soliton, the other Lorenz[2] did a concept of strange attractor(nonperiodic flow) by his simplified model designed to represent the Rayleigh-Bénard convection. Soliton with stable coherent structure represents *order*, while chaos does *disorder* with seemingly turbulent state. Soliton may be twinned with chaos in the light of the Fermi-Pasta-Ulam[3] problem related to the ergodicity due to the nonlinear effects.[4] If soliton and chaos systems with any fluctuations are complementary each other, then one may find order within chaos and chaos within order.[5,6]

It is difficult to find a low-dimensional subspace confining a chaotic attractor for a general infinite-dimensional dynamical system, which is usually described by a set of partial differential equations. In the case of a perturbed soliton system, Nozaki *et al.*[7] succeeded in reducing an infinite-dimensional (soliton) system to a four-dimensional system of ordinary differential equations. However, in general, it is not easy to achieve such a reduction as in a perturbed soliton system. Lorenz , therefore , studied a truncated model which is a three-dimensional system of ordinary differential equations instead of partial differential equations designed to represent the Rayleigh-Bénard convection. Knobloch and co-workers[8,9,10] have extensively studied two slightly different five-dimensional systems of equations which reduce to the Lorenz system when one of the parameters is set to zero. One set of equations is derived from a thermosolutal convection problem, the other from a problem of two-dimensional convection interacting with magnetic fields, which we

call magnetoconvection. They thoroughly reinvestigated magnetoconvection in special regions of jungle of parameters, and found that there was a bifurcation from symmetrical to asymmetrical oscillations followed by a period-doubling leading to *a narrow-band* chaos after the accumulation point.[11] While, in double-diffusive convection, Knobloch, Moore, Toomre and Weiss[12] showed numerically typical strange attractors, power spectra and return-maps in some parameter regions. Knobloch and Weiss,[11] however, did not show them in magnetoconvection. In contrast to double-diffusive convection, Proctor and Weiss[13] concluded that chaotic behaviour has not yet been found in magnetoconvection, though bifurcations to asymmetry have been numerically observed for the full problem described by a set of partial differential equations.[14] Franceshini and Tebaldi[15] studied in detail two infinite sequences of orbits leading to turbulence in a five-mode truncation of the Navier-Stokes equation for a two-dimensional incompressible fluid. Thus these bifurcations from periodic solution may offer a fascinating and tantalizing topic of research for magnetoconvection. They may serve as *a paradigm* for the anomalous diffusion problem of the magnetically confined high temperature plasmas[16] in the light of the contribution of the Lorenz model to nonlinear physics. Because the secondary bifurcations have been numerically observed in the reduced magnetohydrodynamic (MHD) systems related to the anomalous transport in tokamaks.[17,18,19]

The nonlinear interaction between convection and magnetic fields may explain some prominent features on the solar surface. Busse[20] showed that the finite amplitude onset of steady convection became possible at Rayleigh numbers considerably below the values predicted by linear theory.[21] Magnetic fields within sunspots are sufficiently strong to suppress convection on granular and supergranular scales.[21,22] Yet we are far from *a real*

understanding of the dynamical coupling between convection and magnetic fields in stars and magnetically confined high temperature plasmas.[18] Therefore it is of great importance to understand how the energy transport and convection are affected by the imposed magnetic fields; how the Lorentz force affects the pattern of convection in the sunspots and magnetically confined high temperature plasmas. Magnetoconvection exhibits a rich variety of behaviours when the magnetic Prandtl number (the ratio of the magnetic to the thermal diffusivity $\zeta = \eta/\kappa$) is small; $\zeta < 1$. The condition $\zeta < 1$ may be satisfied in the solar convection zone near the sunspots[22] and the magnetically confined high temperature plasmas.[18] The magnetic Prandtl number is significant parameter in magnetoconvection. There is generally an arbitrary choice in the normalization of system, especially with regard to the coefficients of fifth-order model contained ζ. The normalization employed by Knobloch and co-workers[8~11] differs from our normalization in the present paper, and so our fifth-order system is physically different from their system. Our system is a straightforward extension of the Lorenz model[2] in the Boussinesq convection taken into account the Lorentz force. In adition to ζ, moreover, there are four fundamental parameters in magnetoconvection ; σ, r, q and w, where σ is the Prandtl number, r is a normalized Rayleigh number related to the free energy source of system (destabilizing effect), q is a normalized Chandrasekhar number related to the magnitude of the imposed magnetic field (stabilizing effect) and w is a geometrical parameter related to the aspecto-ratio. It is very difficult to find analytical solutions for the fifth-order system of nonlinear ordinary differential equations in the jungle of the five-dimensional parameter space. Therefore a numerical integration enables us to get numerical solutions in certain parameter regions.

The present paper consists of ten sections. In Sec.2 and Sec.3, the derivation of basic equations and linear analysis for two-dimensional magnetoconvection presented by Chandrasekhar[21] are briefly reviewed for the sake of the following sections. Section 4 is a nonlinear stability of steady solutions , which is used to determine the upper limit of the magnetic Prandtl number. In Sec.5, we derive a simplified model to truncate an infinite degrees of freedom of system : a fifth-order system of nonlinear ordinary differential equations with five parameters. In Sec.6, analytical solutions of nonlinear steady convection are given. These steady solutions complicatedly depend on the four parameters excepting σ. In Sec.7, we reduce our system to a normal form equation (the coupled Duffing equation with the van der Pol equation) by a perturbation technique[8] in order to explain qualitatively numerical results. Section 8 and 9 are the numerical results and discussions. Finally, Section 10 contains our conclusions.

2 Basic equations

In this paper we are concerned with a more restricted problem of convection taken account of a nonlinear interaction between the Rayleigh-Bénard convection and an externally imposed magnetic field,within the framework of magnetohydrodynamics(MHD). Here we call its convection magnetoconvection.

Let us consider a horizontally stratified fluid layer of characteristic depth(length) h, referred to a cartesian coordinate system with the z axis pointing vertically upwards and the x axis horizontally rightwards in the two-dimensional case. We start from the following equations:

$$\frac{\partial \mathbf{u}}{\partial t} + (\mathbf{u}\cdot\nabla)\mathbf{u} = -\frac{1}{\rho_0}\nabla p - \frac{\rho}{\rho_0} g\hat{\mathbf{z}} + \frac{1}{\mu_0\rho_0}(\nabla\times\mathbf{B})\times\mathbf{B} + \nu\nabla^2\mathbf{u}, \qquad (2-1)$$

$$\frac{\partial \mathbf{B}}{\partial t} = \nabla\times(\mathbf{u}\times\mathbf{B}) + \eta\nabla^2\mathbf{B}\,, \quad \nabla\cdot\mathbf{B} = 0, \qquad (2-2)$$

$$\frac{\partial T}{\partial t} = -\nabla\cdot(T\mathbf{u}) + \kappa\nabla^2 T, \qquad (2-3)$$

where in the Boussinesq approximation $\nabla\cdot\mathbf{u} = 0$ and $\rho/\rho_0 = 1 - \bar{\alpha}(T - T_0)$; the density ρ is equal to ρ_0 at the reference temperature T_0 , $\bar{\alpha}$ is the coefficient of volume expansion. Here $\mathbf{u}$ is the velocity , T the temperature , $\mathbf{B}$ the magnetic field and p the pressure; the constants ν, η, κ, μ_0 and g are respectively the viscous,magnetic,thermal diffusivities, the magnetic permeability and the acceleration due to gravity, $\hat{\mathbf{z}}$ being a unit vector in the vertial direction. We assume that a fixed temperature difference ΔT is maintained across the layer of fluid (plasma) heated below in an externally imposed magnetic field $\mathbf{B}_0 = B_0\hat{\mathbf{z}}$.

Let us restrict our attention to two-dimensional magnetoconvection in the (x, z) plane, for simplicity. Then the magnetic field can be described by a stream function $\phi(x, z, t)$

and a flux function $A(x,z,t)$ such that

$$\mathbf{u} = (-\frac{\partial \phi}{\partial z},\ 0,\ \frac{\partial \phi}{\partial x}), \tag{2-4}$$

$$\tilde{\mathbf{B}} = (-\frac{\partial A}{\partial z},\ 0,\ \frac{\partial A}{\partial x}), \tag{2-5}$$

where $\mathbf{B} = B_0\hat{\mathbf{z}} + \tilde{\mathbf{B}}$, $\tilde{\mathbf{B}} = \nabla \times (A\hat{\mathbf{y}})$.

Equation(2-2) can be integrated to give

$$\frac{\partial A}{\partial t} + \{\phi, A\} = \eta \nabla^2 A. \tag{2-6}$$

The pressure in eq.(2-1) may be eliminated from the equation of motion by taking its rotation, yielding the vorticity equation :

$$\frac{\partial}{\partial t}\nabla^2\phi + \{\phi, \nabla^2\phi\} = \nu\nabla^4\phi + g\bar{\alpha}\frac{\partial T}{\partial x} + \frac{1}{\rho_0\mu_0}(B_0\frac{\partial}{\partial z}\nabla^2 A + \{A, \nabla^2 A\}). \tag{2-7}$$

A particular configuration is specified by five dimensionless parameters for convection in the region $(0 < x < \lambda h\ ,\ 0 < z < h)$ driven by a vertial temperature difference ΔT; these are the Rayleigh number

$$R = \frac{g\bar{\alpha}\Delta T h^3}{\kappa\nu}, \tag{2-8}$$

the Chamdrasckhar number

$$Q = \frac{B_0^2 h^2}{\mu_0\rho_0\eta\nu}, \tag{2-9}$$

the two Prandtl numberes

$$\sigma = \nu/\kappa\ ,\ \zeta = \eta/\kappa, \tag{2-10}$$

and the normalized cell width λ.

It is convenient to measure lengths in terms of the layer depth h, time in terms of the

thermal relaxation time h^2/κ, temperature in terms of ΔT and magnetic fields in terms of the imposed field B_0. From henceforth all the perturbed quantities will be expressed in dimensionless forms. Then Equations (2-1),(2-2) and (2-3) become

$$\frac{1}{\sigma}(\partial_t \nabla^2 \phi + \{\phi, \nabla^2 \phi\}) = R\frac{\partial \theta}{\partial x} + \nabla^4 \phi + \zeta Q(\frac{\partial}{\partial z}\nabla^2 A + \{A, \nabla^2 A\}), \qquad (2-11)$$

$$\partial_t \theta + \{\phi, \theta\} = \nabla^2 \theta + \frac{\partial \phi}{\partial x}, \qquad (2-12)$$

$$\partial_t A + \{\phi, A\} = \zeta \nabla^2 A + \frac{\partial \phi}{\partial z}, \qquad (2-13)$$

where $\{f, g\} \equiv \frac{\partial f}{\partial x}\frac{\partial g}{\partial z} - \frac{\partial f}{\partial z}\frac{\partial g}{\partial x}$ and $\theta(x, z, t) = T - (1 - z)$.

For convenience we adopt the illustrative stress-free boundary conditions ;

$$\phi = \nabla^2 \phi = 0 \ (x = 0, \lambda \ ; \ z = 0, 1),$$

$$\theta = 0 \ (z = 0, 1), \ \frac{\partial \theta}{\partial x} = 0 \ (x = 0, \lambda),$$

$$A = 0 \ (x = 0, \lambda), \ \frac{\partial A}{\partial z} = 0 \ (z = 0, 1). \qquad (2-14)$$

This choice of boundary conditions has the appealing consequence that the eigenfunctions of the linear stability problem remain proportional to $\exp(i \cdot n\pi z)$ with an integer n.[21] Even in the nonlinear regime the idealized free boundary conditions lead to solutions that are periodic in z.[21]

3 Linear analysis

For the idealized free boundary conditions(2-14) the system is marginally stable to infinitesimal perturbations of the following form;

$$\begin{pmatrix} \phi \\ \theta \\ A \end{pmatrix} \propto \begin{pmatrix} \sin\alpha x \cdot \sin n\pi z \\ \cos\alpha x \cdot \sin n\pi z \\ \sin\alpha x \cdot \cos n\pi z \end{pmatrix} \exp(s^* t), \qquad (3-1)$$

where α is the horizontal wave number.

Substituting(3-1) into (2-11),(2-12) and (2-13), we obtain the cubic characteristic equation

$$\beta^2(s^*+\beta^2)(s^*+\sigma\beta^2)(s^*+\zeta\beta^2)+\sigma\zeta Q\beta^2 n^2\pi^2(s^*+\beta^2)-R\sigma\alpha^2(s^*+\zeta\beta^2)=0, \quad (3-2)$$

where $\beta^2 = \alpha^2 + n^2\pi^2$.

A simple bifurcation ($s^* = 0$) is sometimes referred to an exchange of stabilities, leading to an exponentially growing solution ($Re(s^*) > 0$).

Setting $s^* = 0$ ($R = R^{(e)}$) in (3-2), we have

$$R^{(e)} = \frac{\beta^6 + Qn^2\pi^2\beta^2}{\alpha^2}. \qquad (3-3)$$

It is obvious that for a given value of α^2, $R^{(e)}$ is least when $n = 1$. Therefore we set $n = 1$ henceforth. When $Q = 0$, $R^{(e)} = R_0$,

where

$$R_0(\alpha) = \frac{\beta^6}{\alpha^2} = \frac{(\pi^2+\alpha^2)^3}{\alpha^2}. \qquad (3-4)$$

The minimun value of R_0, namely $27\pi^4/4$, occurs when $\alpha^2 = \pi^2/2$, R_0 is critical Rayleigh number for the onset of convection in the absence of magnetic field.

It is convenient to introduce a more compact notation by defining a normalized Rayleigh number,

$$r = \frac{R}{R_0}, \tag{3-5}$$

and modified parameters τ, s and q,

$$\tau = \beta^2 t,\ s = \beta^{-2} s^*,\ q = \frac{\pi^2}{\beta^4} Q. \tag{3-6}$$

These scalings take up all the geometrical factors so that the characteristic equation(3-2) simplifies to

$$s^3 + (1+\sigma+\zeta)s^2 + [\sigma(1-r+\zeta q) + \zeta(1+\sigma)]s + \sigma\zeta(1+q-r) = 0. \tag{3-7}$$

The condition Eq.(3-3) for a simple bifurcation is now rewritten by $r = r^{(e)}$, where

$$r^{(e)} = 1 + q. \tag{3-8}$$

In addition, there is the possibility of a Hopf bifurcation from the static solution, corresponding to the onset of overstability when s is complex and $Re(s) = 0$ ($s = \pm i\omega_0$), at

$$r = r^{(0)} = (\sigma+\zeta)\left(\frac{1+\zeta}{\sigma} + \frac{\zeta}{1+\sigma} q\right). \tag{3-9}$$

The corresponding frequency of oscillations is given by

$$\omega_0^2 = \frac{\sigma\zeta}{1+\sigma+\zeta}(r^{(e)} - r^{(0)}) = -\zeta^2 + \sigma\zeta\left(\frac{1-\zeta}{1+\sigma}\right) q. \tag{3-10}$$

If $r^{(e)} > r^{(0)}$ and $\zeta < 1$, then ω_0 is real; there is a Hopf bifurcation at $r^{(0)}$ and convection first sets in as an overstable mode. From (3-10), in this case the normalized Chandrasckhar number q must be greater than

$$q_0 = \frac{\zeta}{\sigma}\left(\frac{1+\sigma}{1-\zeta}\right). \tag{3-11}$$

This overstable case ($\omega_0^2 > 0$) is the one of principal concern and astrophysically relevant ($\zeta < 1$). For a perfect fluid ($\kappa = \nu = \eta = 0$) the dimensional frequency of oscillation Ω satisfies

$$\Omega^2 = \frac{\pi^2}{h^2}\left(v_A^2 - \frac{\alpha^2}{\beta^2\pi^2}v_T^2\right), \quad v_A \equiv \left(\frac{B_0^2}{\mu_0\rho_0}\right)^{1/2}, \quad v_T \equiv (gh\bar{\alpha}\Delta T)^{1/2}, \qquad (3-12)$$

where v_A is the Alfvén velocity and v_T the trapped buoyancy velocity due to the temperature-gradient in the Boussinesq approximation. Eq.(3-12) also represents the Alfvén waves when $\Delta T \to 0$. When $\Omega^2 > 0$, magnetoconvection generally sets in as growing periodic (oscillatory) solutions. The ratio of the normalized Rayleigh number to the Chandrasekhar number is given by

$$\frac{r}{q} = \zeta\frac{\alpha^2}{\beta^2\pi^2}\left(\frac{v_T}{v_A}\right)^2. \qquad (3-13)$$

Eq.(3-13) is of course different from the plasma beta in a tokamak plasma[18] because v_T is not the thermal velocity.

4 Nonlinear stability

There exist non-trivial steady solutions corresponding to finite amplitude convection in the neighbourhood of the simple bifurcation at $r^{(c)}$. The linear theory does not, however, tell us whether these solutions will be stable.

First Eqs.(2-11)~(2-13) are written in the compact form :

$$M\,\partial_\tau \Psi + L\,\Psi = N(\Psi,\Psi), \tag{4-1}$$

where

$$\mathrm{M} = \begin{pmatrix} \frac{1}{\sigma R_0}\nabla^2 & 0 & 0 \\ 0 & -r & 0 \\ 0 & 0 & -\zeta\frac{Q}{R_0}\nabla^2 \end{pmatrix}, \tag{4-2}$$

$$\Psi = \begin{pmatrix} \phi(x,z,\tau) \\ \theta(x,z,\tau) \\ A(x,z,\tau) \end{pmatrix}, \tag{4-3}$$

$$\mathrm{L} = \begin{pmatrix} -\frac{1}{R_0}\nabla^4 & -r\partial_x & -\zeta\frac{Q}{R_0}\partial_z\nabla^2 \\ r\partial_x & r\nabla^2 & 0 \\ \zeta\frac{Q}{R_0}\partial_z\nabla^2 & 0 & \zeta^2\frac{Q}{R_0}\nabla^4 \end{pmatrix}, \tag{4-4}$$

$$\mathrm{N}(\Psi,\Psi)=\begin{pmatrix} -\frac{1}{\sigma R_0}\{\phi,\nabla^2\phi\}+\zeta\frac{Q}{R_0}\{A,\nabla^2 A\} \\ r\{\phi,\theta\} \\ \zeta\frac{Q}{R_0}\nabla^2\{\phi,A\} \end{pmatrix}, \qquad (4-5)$$

and $\quad \nabla^2 \equiv \partial_x^2+\partial_z^2.$

Let us introduce a small parameter ε such that

$$\Psi=\sum_{n=1}^{\infty}\varepsilon^n\Psi_n, \qquad (4-6)$$

$$r=r^{(e)}+\sum_{n=1}^{\infty}\varepsilon^n r_n^{(e)}, \qquad (4-7)$$

and

$$L=L_0+\sum_{n=1}^{\infty}\varepsilon^n L_n. \qquad (4-8)$$

If we substitute Eqs.(4-6) and (4-7) into Eq.(4-1), and set the time derivatives to zero, then at leading order in ε, we obtain the following form

$$L_0\,\Psi_1=\begin{pmatrix}0\\0\\0\end{pmatrix}, \qquad (4-9)$$

where from Eqs.(4-4) and (4-7) the self-adjoint differential operator L_0 is defined by

$$\mathrm{L}_0\equiv\begin{pmatrix} -\frac{1}{R_0}\nabla^4 & -r^{(e)}\partial_x & -\zeta\frac{Q}{R_0}\partial_z\nabla^2 \\ r^{(e)}\partial_x & r^{(e)}\nabla^2 & 0 \\ \zeta\frac{Q}{R_0}\partial_z\nabla^2 & 0 & \zeta^2\frac{Q}{R_0}\nabla^4 \end{pmatrix}. \qquad (4-10)$$

Equation(4-9) is just the two-dimensional form of the linear eigenvalue problem, and then the eigenvector is given by

$$\Psi_1 = \begin{pmatrix} \phi_1 \\ \theta_1 \\ A_1 \end{pmatrix} = 2\sqrt{2}\frac{\beta}{\alpha} \begin{pmatrix} \sin\alpha x \cdot \sin\pi z \\ \frac{\alpha}{\beta^2}\cos\alpha x \cdot \sin\pi z \\ \frac{\pi}{\zeta\beta^2}\sin\alpha x \cdot \cos\pi z \end{pmatrix}, \qquad (4-11)$$

where the normalization is chosen for subsequent convenience to simplify the coefficient of $r_2^{(e)}$. Since the operator L_0 is self-adjoint, we have the identity

$$< {}^T\Psi_1 L_0 \Psi_n > = < {}^T\Psi_n L_0 \Psi_1 > = 0, \qquad (4-12)$$

for all natural number n, where the angle brackets denote averages over the domain $(0 \leq x \leq 2\pi/\alpha\ ,\ 0 \leq z \leq 1)$ and the superscript T denotes the transpose of the matrix. To second order in ε, we obtain

$$\mathrm{L_0}\ \Psi_2 = \begin{pmatrix} r_1^{(e)}\partial_x\theta_1 - \frac{1}{\sigma R_0}\{\phi_1,\ \nabla^2\phi_1\} + \zeta\frac{Q}{R_0}\{A_1,\ \nabla^2 A_1\} \\ r^{(e)}\{\phi_1,\ \theta_1\} \\ \zeta\frac{Q}{R_0}\nabla^2\{\phi_1,\ A_1\} \end{pmatrix}. \qquad (4-13)$$

From Eq.(4-11) it follows that the two Jacobians in the first row on the right-hand side of (4-13) are identically zero. The compatibility condition on this inhomogeneous equation is obtained by (4-12) to (4-13): it then follows that $r_1^{(e)} = 0$. If we impose the orthogonality condition

$$< {}^T\Psi_1 \Psi_n > = 0 \qquad (n \neq 1), \qquad (4-14)$$

then the solution of (4-13) is

$$\Psi_2 = \begin{pmatrix} \phi_2 \\ \theta_2 \\ A_2 \end{pmatrix} = \begin{pmatrix} 0 \\ -\frac{1}{\pi}\sin 2\pi z \\ \frac{\pi^2}{\zeta^2\alpha^3}\sin 2\alpha x \end{pmatrix}. \qquad (4-15)$$

At third order in ε , we have

$$\mathrm{L}_0\Psi_3 = \begin{pmatrix} r_2^{(e)}\partial_x\theta_1 + \zeta\frac{Q}{R_0}(\{A_1,\, \nabla^2 A_2\} + \{A_2,\, \nabla^2 A_1\}) \\ r^{(e)}\{\phi_1,\, \theta_2\} \\ \zeta\frac{Q}{R_0}\nabla^2\{\phi_1,\, A_2\} \end{pmatrix}. \qquad (4-16)$$

The solvability condition yields, from (4-12) and (4-16),

$$r_2^{(e)} = 1 + q + \frac{2\pi^2(\alpha^2 - \pi^2)}{\zeta^2\alpha^2\beta^2}q. \qquad (4-17)$$

This result was originally obtained by Veronis[23] and quoted by Weiss.[14] It follows that the finite amplitude solution is stable if $r_2^{(e)} > 0$ and unstable if $r_2^{(e)} < 0$. Thus the finite amplitude solutions favor a vertically elongated cell with $\zeta \ll 1$ and $w < 2$.

Equation(4-17) is rewritten as follows :

$$r_2^{(e)} \leq 1 + \{1 + \frac{\sqrt{2}}{\zeta^2}(1 - \frac{1}{\sqrt{2}})^2\}q. \qquad (4-18)$$

From Eq.(4-18), we can estimate the upper limit of ζ ($\zeta^2 \leq \sqrt{2}(1 - 1/\sqrt{2})^2$) :

$$\zeta \leq 0.35\ (\ \lambda \sim 0.64\ ). \qquad (4-19)$$

Hereafter we take account of the above condition (4-19) with respect to ζ.

5 Reduction to a simplified model

We are interested in the behaviour of nonlinear solutions in the neighbourhood of bifurcations from static equilibrium. Although we should solve analytically the partial differential equations(2-1), (2-2) and (2-3) (or (2-11), (2-12) and (2-13)), it is difficult, in general, to do so. Hence it is instructive, also convenient, to introduce a truncated simplified model with the following properties[8~11,13] :

i. the bifurcations at $r^{(0)}$ and $r^{(c)}$ are identical with those for Eqs.(2-11)~(2-13) ;

ii. to second order in ε the finite amplitude solutions are identical with those for Eqs. (2-11)~(2-13) ;

iii. the solutions are bounded as functions of time for each value of the normalized Rayleigh number r ;

iv. the form of the stable parts of the branches of periodic and steady solutions is qualitatively similar to that for Eqs.(2-11)~(2-13).

These aims can be achieved by expressing ϕ, θ, A in terms of a restricted set of spatial models and obtaining a system of ordinary differential equations that governs thier evolution in time.[23] Thus we write

$$\begin{aligned} \phi &= a(\tau)\phi_1, \\ \theta &= b(\tau)\theta_1 + c(\tau)\theta_2, \\ A &= d(\tau)A_1 + e(\tau)A_2, \end{aligned} \tag{5-1}$$

where ϕ_i , θ_i and A_i $(i = 1,2)$ are given by (4-11) and (4-15). It should be noted that $a(\tau)$ represents the first order velocity perturbation, while $b(\tau)$, $c(\tau)$ and $d(\tau)$, $e(\tau)$

are measures of the first and second order perturbations to the temperature and to the magnetic flux function, respectively.

We then substitute these expressions into Eqs.(2-11)~(2-13) and neglect all terms generated that involve higher harmonics so as to obtain the system

$$\dot{a} = \sigma\left[-a + r\cdot b - q\cdot d\left(1 + \frac{w(3-w)}{\zeta^2(4-w)}e\right)\right], \qquad (5-2a)$$

$$\dot{b} = -b + a - ac, \qquad (5-2b)$$

$$\dot{c} = w(-c + ab), \qquad (5-2c)$$

$$\dot{d} = -\zeta(d-a) - \frac{w}{\zeta(4-w)}ae, \qquad (5-2d)$$

$$\dot{e} = -\zeta(4-w)(e-ad), \qquad (5-2e)$$

where w represents the geometrical parameter related to the aspect-ratio

$$w = 4\pi^2/\beta^2 \quad (0 < w < 4), \qquad (5-3)$$

and dots denote differentiation with respect to τ.

This type of model was first presented by Veronis[24] in studying the effects of solutions and rotation on convection. Our model is similar to that followed by Knobloch, Weiss and da Costa[9] but the normalization is different from Refs. $8 \sim 11$ since thier eigenvectors did not satisfy Eq.(4-9) : the coefficient of the linear eigenfunction A_1 was $2\sqrt{2}/\beta$ instead of $2\sqrt{2}\frac{\pi}{\zeta\alpha\beta}$.

The divergence of the flow in phase can be calculated from Eq.(5-2),

$$\frac{\partial}{\partial a}\dot{a} + \frac{\partial}{\partial b}\dot{b} + \frac{\partial}{\partial c}\dot{c} + \frac{\partial}{\partial d}\dot{d} + \frac{\partial}{\partial e}\dot{e} = -[1 + \sigma + w + \zeta(5-w)], \qquad (5-4)$$

is always negative since $0 < w < 4$. So trajectories are attracted to a set of measure zero in the phase space; they may be attracted to a limit cycle, a fixed point (corresponding to a steady convection) and a strange attractor, which has not yet been found.

The system(5-2) possesses an important symmetry, for it is invariant under the transformation

$$(a, b, c, d, e) \rightarrow (-a, -b, c, -d, e) \qquad (5-5)$$

When $q = 0$ the first three equations of (5-2) decouple from the rest and can be transformed to the Lorenz model,[2] which has been extensively investigated.[25]
Although the system (5-2) can display all the behaviour associated with the Lorenz model, we shall be concerned with solutions in a different regime, for values of r sufficiently small that the Lorenz attractor has not yet appeared.

It is convenient to introduce a normalized heat flux, given by the Nusselt number

$$Nu \equiv \frac{1}{\lambda}\int_0^1 \left(1 - \frac{\partial\theta}{\partial z}\right) dx. \qquad (5-6)$$

The Nusselt number is defined by the ratio of the total heat flux to the flux that there would be in the absence of convection. For a purely conducting solution we have $Nu = 1$ and for a finite amplitude convection, from Eqs. (4-15) and (5-1),

$$Nu = 1 + 2\,c\,(\tau), \qquad (5-7)$$

where the Nusselt number can be evaluated at $z = 0$ or $z = 1$.

6 Steady convection

The simplified system (5-2) is more tractable than full problem (4-1)~(4-6). Steady finite amplitude solutions can be readily obtained from (5-2);

$$b = \frac{a}{1+a^2},\ c = \frac{a^2}{1+a^2},\ d = \frac{\mu a}{\mu + a^2},\ e = \frac{\mu a^2}{\mu + a^2} \qquad (6-1)$$

where the parameter μ is defined by

$$\mu = \frac{\zeta^2(4-w)}{w} \qquad (6-2)$$

and

$$r = 1 + a^2 + \frac{\mu(1+a^2)[\mu + (4-w)a^2]}{(\mu + a^2)^2} q \qquad (6-3)$$

It should be noted that μ is always positive since $0 < w < 4$ and that the solution of (6-3) do not depend on σ. Equation(6-3) is a cubic in terms of a^2 , which has two limits;

(i) the case of small a^2 ($a^2 \sim 0$)

$$r = 1 + q = r^{(e)}$$

(ii) the case of large a^2 ($a^2 \gg 1$)

$$r \sim a^2 + \zeta^2 \frac{(4-w)^2}{w} q$$

From above limits, in the case of small ζ and large a^2, we have

$$|a| \sim \sqrt{r}. \qquad (6-4)$$

The stability of the steady solutions can be linearizing equations (5-2) about the steady solutions (6-1) and (6-3), and looking for solutions that grow like $\exp s\tau$. The growth rate

is given by the roots of a quintic dispersion relation

$$s^5 + d_1 s^4 + d_2 s^3 + d_3 s^2 + d_4 s + d_5 = 0, \qquad (6-5)$$

where

$$d_1 = 1 + \sigma + w + \zeta(5-w),$$

$$\begin{aligned} d_2 = \sigma\zeta^2(4-w)\Bigg[&\frac{\zeta a^2 + \mu(\zeta+\sigma+w+1)}{\sigma\mu\zeta} + \frac{\sigma(1+w+\zeta)+a^2+w+\zeta+\zeta w}{\sigma(4-w)\zeta^2} \\ &+\frac{\mu q\{wa^4 + a^2(16-8w+w\mu-w^2)+\mu\}}{\zeta(a^2+\mu)^2(4-w)} - \frac{r}{1+a^2}\cdot\frac{1}{\zeta^2(4-w)}\Bigg], \end{aligned}$$

$$\begin{aligned} d_3 = \sigma\zeta^2(4-w)\Bigg[&\frac{(\mu+a^2)(\sigma+w-1)}{\sigma\mu} + \frac{a^2+\sigma+w(\sigma+1)}{\sigma\zeta} \\ &-\frac{a^2q\{a^2\zeta(3-w)-\mu(3+9\zeta+3\zeta w+2w)\}}{(a^2+\mu)^2\zeta} - \frac{r\{w(1-a^2)+\zeta(5-w)\}}{(1+a^2)(4-w)\zeta^2} \\ &+\frac{a^2(\sigma+\zeta)+\sigma(w+w\zeta+\zeta)+w\zeta}{\sigma(4-w)\zeta^2} + \frac{\mu q\{a^2(3-2w+w^2)+1+w\mu\}}{(a^2+\mu)^2(4-w)\zeta} - \frac{q(a^2-\mu)}{a^2+\mu}\Bigg], \end{aligned}$$

$$\begin{aligned} d_4 = \sigma\zeta^2(4-w)\Bigg[&\frac{(\sigma+a^2)(\mu+a^2)+w(\mu-a^2)(\sigma+1)}{\sigma\mu} + \frac{(a^2+w)(5-w)}{(4-w)\zeta} \\ &+\frac{\mu q\{a^4(3-5w+w^2)+a^2(1+16w-8w^2+w^4)+w\mu\}}{(a^2+\mu)(4-w)\zeta} \\ &-\frac{q\{a^4(4+w-w^2-3\mu)+3a^2(w+w\mu+w^2\mu-3\mu)-\mu^2-w\mu^2\}}{(a^2+\mu)^2} \\ &-\frac{r(\mu+a^2)}{(1+a^2)\mu} - \frac{rw(1-a^2)(5-w)}{(1+a^2)(4-w)\zeta}\Bigg], \end{aligned}$$

$$\begin{aligned} d_5 = \sigma\zeta^2(4-w)\Bigg[&\frac{(a^2+w)(\mu+a^2)}{\mu} - \frac{a^2q\{a^4(1-w)+a^2(3w+3w\mu-w^2-3\mu)-9\mu w\}}{(a^2+\mu)^2} \\ &-\frac{q(a^2-\mu)(a^2+w)}{a^2+\mu} - \frac{rw(1-a^2)(\mu+a^2)}{(1+a^2)\mu}\Bigg]. \end{aligned}$$

The coefficient d_1 is related to Eq.(5-4). The dependence of the growth rate on the amplitude is not clear from Eq.(6-5) since the coefficients $d_i (i = 2 \sim 5)$ contained the Rayleigh number are generally so complicated function of the amplitude a^2. The growth rate may be obtained by solving Eq.(6-5) numerically. However, in the present paper, we proceed to the direct numerical computations of Eq.(5-2), rather than studying Eq.(6-5) in detail.

7 A normal form equation

It is difficult to find analytically the general nonlinear solutions of Eq.(5-2). In the neighbourhood of the Hopf bifurcation point $r^{(0)} \leq r^{(c)}$, however, it is possible to obtain finite-amplitude periodic solutions by means of a perturbation technique.[8]

We assume that r is close to $r^{(0)}$ and $r^{(c)}$, and that q is also close to q_0;

$$r = \frac{\sigma+\zeta}{\sigma(1-\zeta)} + m\cdot\varepsilon^2 \qquad (7-1)$$

$$q = \frac{\zeta(1+\sigma)}{\sigma(1-\zeta)} + \varepsilon^2 \qquad (7-2)$$

where m is an arbitrary parameter $m \sim O(1)$. Substituting (7-1) and (7-2) into (5-2), taking account of the ordering (4-6), we have

$$\varepsilon a' = \sigma\left[-a + b\left\{\frac{\sigma+\zeta}{\sigma(1-\zeta)} + m\cdot\varepsilon^2\right\} - d\left\{\frac{\zeta(1+\sigma)}{\sigma(1-\zeta)} + \varepsilon^2\right\}\left(1 + \frac{3-w}{\mu}e\cdot\varepsilon^2\right)\right], \quad (7-3a)$$

$$\varepsilon b' = -b + a(1 - c\cdot\varepsilon^2), \qquad (7-3b)$$

$$\varepsilon c' = w(-c + ab), \qquad (7-3c)$$

$$\varepsilon d' = -\zeta\left(d - a + \frac{1}{\mu}ae\cdot\varepsilon^2\right), \qquad (7-3d)$$

$$\varepsilon e' = -\zeta(4-w)(e-ad), \qquad (7-3e)$$

where the prime denotes differentiation with respect to the time $t = \varepsilon\tau$. The leading order amplitudes yield

$$a \simeq b \simeq d\,,\ c \simeq ab\,,\ e \simeq ad. \qquad (7-4)$$

Here we set

$$b = a + \varepsilon g\,,\ d = a + \varepsilon h\,,\ c = a^2 + \varepsilon k\,,\ e = a^2 + \varepsilon l, \qquad (7-5)$$

where h is the perturbed term of the magnetic flux $d(t)$, but the context should prevent any confusion with the fluid layer of characteristic length. From (7-3b) and (7-5), we have

$$g = -b' - \varepsilon ac. \tag{7-6}$$

Eliminating b from (7-6), with repeated use of (7-5), we get

$$g = -a' + \varepsilon(a'' - a^3) - \varepsilon^2(ak + a''' - 3a^2a') + O(\varepsilon^3). \tag{7-7}$$

The same procedure applied to k gives

$$k = -aa'\left(1 + \frac{2}{w}\right) + O(\varepsilon). \tag{7-8}$$

Substituting (7-8) into (7-7), we obtain

$$g = -a' + \varepsilon(a'' - a^3) - \varepsilon^2\left\{a''' - \left(4 + \frac{2}{w}\right)a^2a'\right\}. \tag{7-9}$$

Similarly we have from (7-5),

$$h = -\frac{1}{\zeta}a' + \frac{\varepsilon}{\zeta^2}\left(a'' - \frac{w}{4-w}a^3\right) - \frac{\varepsilon^2}{\zeta^3}\left\{a''' - \frac{w}{4-w}\left(4 + \frac{2}{4-w}\right)a^2a'\right\}, \tag{7-10}$$

$$l = -\frac{1}{\zeta}\left(1 + \frac{2}{4-w}aa'\right). \tag{7-11}$$

Substitution of (7-8)~(7-11) into (7-3a) yields

$$\begin{aligned}\varepsilon\frac{a'}{\sigma} = -a + \left\{\frac{\sigma+\zeta}{\sigma(1-\zeta)} + m\varepsilon^2\right\}\left[a - \varepsilon a' + \varepsilon^2(a'' - a^3) - \varepsilon^3 A\right] \\ -(q_0 + \varepsilon^2)\left\{a - \frac{\varepsilon}{\zeta}a' + \frac{\varepsilon^2}{\zeta^2}\left(a'' - \frac{w}{4-w}a^3\right) - \frac{\varepsilon^3}{\zeta^3}\tilde{A}\right\} \\ \times\left[1 + \varepsilon^2\frac{3-w}{\mu}\left\{a^2 - \frac{\varepsilon}{\zeta}\left(1 + \frac{2}{4-w}\right)aa'\right\}\right],\end{aligned} \tag{7-12}$$

where

$$A = a''' - \left(4 + \frac{2}{w}\right)a^2a' \ , \ \tilde{A} = a''' - \frac{w}{4-w}\left(4 + \frac{2}{4-w}\right)a^2a'.$$

Finally we obtain a normal form equation

$$a'' - \varepsilon(c_1 - c_2 a^2)a' + \zeta c_1 a + c_3 a^3 = \varepsilon c_4 a''' + O(\varepsilon^2), \qquad (7-13)$$

where

$$\begin{aligned}
c_1 &= \frac{\sigma(1-m)}{1+\sigma+\zeta}, \\
c_2 &= \frac{\zeta\sigma}{1+\sigma+\zeta}\left\{\frac{1+\sigma}{\sigma(1-\zeta)}\left(\frac{\zeta}{\mu}\right)^2(5-w) - \frac{2(\sigma+\zeta)}{\sigma(1-\zeta)}\left(2+\frac{1}{w}\right)\right\} \\
&= \frac{\sigma}{1+\sigma+\zeta}\left\{\left(\frac{\zeta}{\mu}\right)^2(5-w) - \frac{2(\sigma+\zeta)}{1+\sigma}\left(2+\frac{1}{w}\right)\right\} q_0, \\
c_3 &= \frac{1}{1+\sigma+\zeta}\left\{\frac{\zeta(\sigma+\zeta)}{1-\zeta} + \zeta\sigma\frac{3-w}{\mu} - \frac{\zeta^2(1+\sigma)}{(1-\zeta)\mu}\right\} \\
&= \frac{\zeta\sigma}{1+\sigma+\zeta}\left\{r_2^{(e)} + \frac{3-w}{\mu}(1-q_0)\right\}, \\
c_4 &= \frac{\zeta\{1+\sigma+\zeta+\zeta(\zeta+\sigma)\}}{1+\sigma+\zeta}.
\end{aligned}$$

Here the coefficient c_2 represents physically a measure of stabilizing effects and c_3 a measure of total destabilizing effects. Equation (7-13) is called the coupled Duffing equation with the van der Pol type equation (CDP) , and may explain some qualitative properties of Eq.(5-2). The coefficients $c_i\,(i = 1 \sim 4)$ of Eq.(7-13) are different from those of Refs. 8, 26 and 27 for lack of the second term of c_3, $(3-w)(1-q_0)/\mu$, and so forth. Also, Eq.(7-13) has two limits ;

(i) the case of small a^2, corresponding to small m $(0 < m < 1)$;

$$a'' - \varepsilon(|c_1| - c_2 a^2)a' + \zeta|c_1|a \simeq 0, \qquad (7-14)$$

(ii) the case of large a^2 $(m > 1)$;

$$a'' - \zeta|c_1|a + c_3 a^3 \simeq O(\varepsilon), \qquad (7-15)$$

where c_3 is assumed to be positive and $O(1)$, in fact, $c_3 = 2.41$ for the typical parameters with $\zeta = 0.1$, $\sigma = 1$ and $w = 0.8$. When $c_1 = 0$ ($m = 1$), Eq.(7-13) has a double-zero eigenvalue, we call its point a codimension-2 point X,[28] which was considered by Takens[29] and Bogdanov.[30] Particularly, when $\varepsilon \to 0$, Eq.(7-13) reduces to the Duffing equation, which has a single-parameter family of periodic solutions that depend on the value of the Hamiltonian

$$H_0(a, a') = \frac{1}{2}(a')^2 - \frac{1}{2}\zeta|c_1|a^2 + \frac{1}{4}c_3 a^4. \qquad (7-16)$$

The periodic solutions of the Duffing equation can be expressed in terms of Jacobian elliptic functions, which were extensively discussed by Knobloch and Proctor.[8]

Since the coefficient c_1 becomes negative for the large amplitudes, the normal form equation (7-13) possesses a homoclinic orbit and a hyperbolic saddle point where the stable manifold W^s coincides with its unstable manifold W^u. The unperturbed system (7-16) has two homoclinic orbits $\Gamma_0^{\pm}$ which can be determined by integration from the Hamiltonian H_0, and also two centers E_+ and E_-. Any small perturbation will lead to a change of the stable and unstable manifolds of the saddle point so that the curve no longer closes because a homoclinic orbit is not structurally stable.[28] A small perturbation can result in the emergence of an unstable fixed point and a stable fixed point emanating from the centers E_+ and E_-. If the stable and unstable manifolds intersect, then a map in a Poincaré section Σ_{t_0} leads to the Smale's horseshoe map.[31] The existence of such a map is equivalent to the impossibility of long-term prognoses. The behaviour of stable and unstable manifolds can be determined by calculating the Melnikov function[28] for the perturbed systems. The Melnikov function is the $O(\varepsilon)$-term in a power series expansion

of ε for the distance between W_ε^s and W_ε^u. From Eq.(7-15), we have two centers

$$E_\pm = (\pm\sqrt{\zeta \mid c_1 \mid / c_3}\,, 0). \tag{7-17}$$

While, Eq.(7-16) yields

$$a(t) = \pm\left(\frac{2\zeta \mid c_1 \mid}{c_3(2-k)}\right)^{1/2} \mathrm{dn}\left[\left(\frac{\zeta \mid c_1 \mid}{2-k}\right)^{1/2} t\,, k\right], \tag{7-18}$$

where k is the elliptic modulus ($0 \leq k < 1$). When $k \to 1$, the double homoclinic orbits $\Gamma_0^\pm$ are given by

$$(a_0(t), a_0'(t)) = \left(\pm\sqrt{\frac{2\zeta|c_1|}{c_3}}\,\mathrm{sech}\sqrt{\zeta|c_1|}\,t,\ \mp\zeta|c_1|\sqrt{\frac{2}{c_3}}\,\mathrm{sech}\sqrt{\zeta|c_1|}\,t\cdot\tanh\sqrt{\zeta|c_1|}\,t\right). \tag{7-19}$$

The Melnikov function for Eq.(7-13) can be defined by

$$M(t_0) = \varepsilon\int_{-\infty}^{\infty} a_0'(t)\left\{|c_1|a_0'(t) - c_2a_0^2(t)a_0'(t) + c_4a_0'''(t)\right\}dt. \tag{7-20}$$

From Eqs.(7-19) and (7-20), we obtain an expression for the Holmes-Melnikov boundary[32] where the bifurcation situation (occurrence of a double saddle connection) is given by $M(t_0) \equiv 0$,

$$5c_3 - 4\zeta c_2 - 7\zeta c_3 c_4 = 0. \tag{7-21}$$

In the neighbourhood of the codimension-2 point X, it is convenient to introduce a renormalized Chandrasekhar number $\tilde{q}$ and a renormalized Rayleigh number $\tilde{r}$ as follows :

$$\tilde{q} = \left\{ \left(\frac{\zeta}{\mu}\right)^2 (5-w) - \frac{2(\sigma+\zeta)}{1+\sigma}(2+\frac{1}{w}) \right\} q_0, \qquad (7-22)$$

$$\tilde{r} = r_2^{(c)} + \frac{3-w}{\mu}(1-q_0). \qquad (7-23)$$

Here $\tilde{q}$ or $\tilde{r}$ is a kind of renormalized expression contained the parameters ζ, σ and w in the neighbourhood of the codimension-2 point X. Substitution of (7-22) and (7-23) into (7-21) yields

$$5\,\tilde{r} \;-\; 4\,\tilde{q} \;=\; 7\zeta^2 \frac{\{1+\sigma+\zeta+\zeta(\zeta+\sigma)\}}{1+\sigma+\zeta}\,\tilde{r}. \qquad (7-24)$$

Since the right-hand side of Eq.(7-24) is negligible because $\zeta^2 \ll 1$, Eq.(7-24) becomes :

$$\tilde{q} = B_{HM}\,\tilde{r}, \qquad (7-25)$$

where B_{HM} is related to the slope of the renormalized Holmes-Melnikov boundary and a universal constant in the neighbourhood of the codimension-2 point X : $B_{HM} = 5/4$.

8 Numerical results

The fifth-order system (7-3) is equivalent to Eq.(5-2) since the small parameter ε can be set to unity for the truncated model. Therefore we may use t as time variable instead of τ. The choice of parameter-regions in the five-dimensional parameter space is crucial to the numerical integrations. Although the periodic solutions depend on all the five parameters, the steady solutions are independent of the Prandtl number σ. These steady solutions still complicatedly depend on the four parameters.

Since the aim of the present paper is to investigate how the branch of steady solutions is nonlinearly affected by the presence of finite amplitude periodic solutions, first of all, let us consider the relation between the Rayleigh number and the amplitude of steady solutions, which is given by Eq.(6-3). This relation plays an important role in the search after chaos. Figures 1 $\sim$ 6 are the amplitude-Rayleigh number diagrams of steady solutions of one coordinate $a(t)$ for the different parameters. They show that the sign of $r_2^{(e)}$ given by Eq.(4-17) does not always determine whether the branch of steady solutions is supercritical or subcritical in the magnetoconvection though it has vital information about the steady solutions in the duble-diffusive systems.[8] Figure 1 (a)$\sim$(g) indicates a relation between the amplitude of steady solutions and the Rayleigh number with $\zeta = 0.1$ and $w = 0.8$ when q is increased. In the case of Fig. 1 (a), the simple bifurcation point $r^{(e)}$ is supercritical due to $q = 0$ and equivalent to that of the Lorenz model. As q is increased, the branch of steady solutions becomes subcritical at $r^{(e)}$, as is shown in Fig. 1 (b) $\sim$ (g). From Eq.(5-3) and $\lambda = 2\pi/\alpha$, we have the following relations between w and λ ; $w = 0.1081$ ($\lambda = 1/6$), $w = 0.2353$ ($\lambda = 1/4$), $w = 0.8$ ($\lambda = 1/2$), $w = 2$ ($\lambda = 1$), $w = 8/3$ ($\lambda = \sqrt{2}$), $w = 3.2$ ($\lambda = 2$), $w = 3.6$ ($\lambda = 3$), $w = 3.7647$ ($\lambda = 4$).

Figure 2 (a)$\sim$(g) indicates a relation between the amplitude of steady solutions and the Rayleigh number with $\zeta = 0.1$ and $q = 5$ when w is increased. As w is increased, the branch of steady solutions becomes subcritical from supercritical at $r^{(e)}$. Figure 3 (a)$\sim$(g) indicates a relation between the amplitude of steady solutions and the Rayleigh number with $w = 0.8$ and $q = 5$ when ζ is increased. As ζ is increased, the branch of steady solutions becomes supercritical from subcritical at $r^{(e)}$. Figure 4 (a)$\sim$(g) indicates a relation between the amplitude of steady solutions and the Rayleigh number with $w = 2$ and $q = 5$ when ζ is increased. As ζ is increased, the branch of steady solutions becomes subcritical for $\zeta < 0.6$ and supercritical for $\zeta \geq 0.6$, which we are not concerned with, because of the condition (4-19). Similarly, Fig. 5 (a)$\sim$(g) indicates a relation between the amplitude of steady solutions and the Rayleigh number with $w = 3.2$ and $q = 5$ when ζ is increased. Figure 6 (a)$\sim$(g) indicates a relation between the amplitude of steady solutions and the Rayleigh number with $w = 3.6$ and $q = 5$ when ζ is increased. As ζ is increased, the branchs of steady solutions in Figs.5 and 6 are always subcritical for $\zeta < 0.5$.

There is a Hopf bifurcation at $r^{(0)}$ when $\omega_0^2 > 0$ with $r^{(0)} < r^{(e)}$ and $\zeta < 1$. The branch of linear periodic solution bifurcates from the static solution at $r = r^{(0)}$. However, in general, nonlinear periodic solutions with five parameters cannot be found analytically, and we therefore integrate Eq.(5-2) numerically as an initial-value problem. As an initial condition, we take usually $a = 0.1$ and $b = c = d = e = 0$ at $t = 0$. Since numerical results do not depend at all on our choice of initial condition if we ignore initial transient period. We use the fourth-order Runge-Kutta scheme with appropriately chosen timesteps ($\Delta t = 0.01,\ 0.05,\ 0.1$).

Since our fifth-order system reduces to the Lorenz system in the limit of the absence of magnetic field ($q = 0$), we can expect that our system exhibit a similar property to the Lorenz model. In fact, Fig.7(a) indicates a typical stange attractor of the Lorenz type projected onto the bc-plane from the five dimensional space (a, b, c, d, e) with the typical parameters: $\zeta = 0.5$, $\sigma = 10$, $w = 2$, $q = 5$ and $r = 30$. Although this strange attractor is similar to the Lorenz attractor, as is shown in Fig.7(b), its return-map of the succesive maxima of $c(t)$ is not equal to the Lorenz map because of the presence of magnetic field ($q = 5$) and becomes equivalent to the Lorenz map in the limit $q \to 0$ (See Fig.7(c)). We are interested in the different bifurcations from those studied in the Lorenz system, and hereafter we are restricted to the case of the smaller Prandtl number and the sufficiently small Rayleigh number that the Lorenz attractor has not yet appeared.

We specify the amplitude of the periodic solution by the maximum of $|a|$ after the solution has settled to a periodic state. The periodic branch can then be represented by plotting the amplitude as a function of the normalized Rayleigh number r. The relationship between the periodic and the steady solutions is shown in Fig. 8, which is the amplitude-Rayleigh number diagram with $\zeta = 0.1$, $\sigma = 1$, $w = 0.8$ and $q = 5$, where we have $r^{(0)} = 1.485$ from Eq.(3-9) and $q_0 = 0.222$ from Eq.(3-11). In Figures $8 \sim 13$, these four parameters(ζ, σ, w, q) are fixed. According to the linear theory reviewed in Sec.3, the branch of periodic solutions denoted by the open circles appears at $r \gtrsim r^{(0)} = 1.485$. The amplitudes of periodic solution are small when r is close to $r^{(0)}$, and so the periodic solution behaves like a linear pendulum, because the normal form equation (7-13) becomes $a'' + \zeta|c_1|a \sim 0$ when $\varepsilon \to 0$. For the linear stage ($r^{(0)} \lesssim r \lesssim 1.7$), the phase portrait projected onto the $a - a'$ plane from the five-dimensional space is a limit cycle of small

ellipse. As r is increased with the fixed parameters : $\zeta = 0.1$. $\sigma = 1$, $w = 0.8$ and $q = 5$, the amplitude of periodic solutions grows and becomes more obviously nonlinear. For the nonliear stage ($1.7 \lesssim r \lesssim 3.0$), the limit cycle of sinusoidal oscillation is transformed into that of the relaxation oscillation described by the van der Pol equation, where the transition to it can be qualitatively explained by Eq.(7-14). For the strong nonlinear stage ($3.0 \lesssim r \lesssim 3.4$), the limit cycle of the relaxation oscillation is transformed into that of the elliptic functional oscillation described by the Duffing equation, where this transition can be also explained by Eq.(7-15). However, even in this stage, the amplitude of the magnetic flux $d(t)$ is always small because $|d| \sim O(\zeta^2)$ when $\zeta \ll 1$, if the amplitude of periodic solution can be estimated by that of steady solution Eq.(6-1). It followed from (7-14) that $d(t)$ is approximately described by the van der Pol equation. At $r = 3.43$, a transition from the periodic solution to chaos (denoted by ▲) is found through the period-doubling cascade, as is shown in Fig. 9 (a) $\sim$ (j), plotted by the one-dimensional Poincaré return-map of the successive maxima of $a(t)$: $a_{n+1} = f(a_n)$. These results were checked by obtaining more accurate solutions with $\Delta t = 0.01$ and $1 \times 10^5 \sim 1 \times 10^6$ iterations. We find the Period-5 window at $r \sim 3.437$ (g), the unfolded chaos at $r = 3.44$ (h), repeatedly the Period-5 window at $r = 3.445$ (i) and the more unfolded chaos at $r = 3.446$ (j). At $r \sim 3.448$, the Period-2 appears again, and the branch of chaotic solutions terminates on that of the nonlinear steady solutions which can be calculated from Eq.(6-3).

Two types of strange attractors are shown in Fig.10 (a), which is corresponding to Fig. 9 (h) with $r = 3.44$. One type of these two strange attractors is projected onto

the $a - a'$ plane and the other type projected onto the $d - d'$ plane from one attractor in the five-dimensional space of the fifth-order system. It should be noted that each phase portrait of the $a - a' \sim e - e'$ planes represents a part of projections from the one common attractor in the five-dimensional space. It folllows from Eq.(7-13) that this attractor possesses the properties described by both the Duffing equation and the van der Pol equation. The phase portrait of the $a - a'$ plane is Duffing-like and that of the $d - d'$ plane van der Pol-like. In regard to the Duffing equation, Ueda [33] has studied the forced Duffing equation most extensively and shown its strange attractor, which is different from our attractors because he considered the external force of forced oscillation. The Period-5 window is found with $r = 3.4375$, corresponding to Fig.9(g) because this window is stable for $3.437 \lesssim r \lesssim 3.4375$. A set of time-evolution of typical chaotic solutions is shown in Fig.11,corresponding to Fig.9(h) and Fig.10(a). It can be clearly observed that a measure of magnetic flux d(t) shows the relaxation oscillation described by the van der Pol equation because of $|d(t)| \ll |a(t)| \sim O(1)$ where $d(t)$ is the first order perturbation to the magnetic flux function. Also the Nusselt number can be evaluated from Eq.(5-7) : $Nu \sim 2.4$.

There is no periodic solution without the magnetic fluctuations. Although $d(t)$ is small for the typical parameters, it plays a vital role in Eq.(5-2). In comparison with Fig.7(a), Fig.12 shows considerable difference in the phase portrait projected onto the $b - c$ plane. A Poincaré section of magnetic flux $d(t)$ projected onto the $d - d'$plane is shown in Fig.13, which is corresponding to Fig.9 (h) and Fig.10 (a). Figure 14 shows the stability diagram for the Chandrasekhar number plotted by the log-scale versus the Rayliegh number plotted by the linear-scale with $\zeta = 0.1$, $\sigma = 1$ and $w = 0.8$. The X

point is defined by $(r_0^{(0)}, q_0)$, where $r_0^{(0)}$ denotes the $r^{(0)}$ with $q = q_0$ and q_0 obtained from Eq.(3-11):

$$r_0^{(0)} = 1.22\ ,\ q_0 = 0.22.$$

In region I, all perturbations are damped on a linear basis, in region II the periodic modes are stable, and in region III the steady convections are stable. The linear stability boundary XV is given by Eq.(3-9). It is *extremely* difficult to obtain analytically a nonlinear stability boundary XW. Therefore we show the nonlinear stability boundary XW obtained by numerical integrations:

$$q = q_0 + B_N\,(r - r_0^{(0)}), \qquad (8-1)$$

where B_N is related to the slope of the boundary obtained numerically (q is plotted by the log-scale in Fig. 14) : $B_N \sim 2$ in this case. For some parameters we can find a chaotic solution (denoted by ▲) on the nonlinear stability boundary XW extrapolated from the point X. The amplitude-Chandrasekhar number diagram is shown in Fig.15. Figure 15(a) is corresponding to L_1 and Fig.15(b) to L_2 in Fig.14. Also, Fig. 8 is corresponding to L_3 in Fig. 14. There is no chaos on the XW for $r = 2$ (L_2): it is denoted by △ . Figure 15 (b) is consistent with the numerical simulations on the original partial differential equations (2-11) $\sim$ (2-13).[14] We find a chaotic solution with $q = 5$ in Fig.15(a). The fixed parameters used in Figs.16$\sim$18 are $\zeta = 0.26$, $\sigma = 1$, $w = 0.8$ and $q = 5$. A sequence of heteroclinic bifurcations[25] from periodic solution is shown in Fig.16 (a)$\sim$(h) projected onto the $a - a'$ plane when r is increased. The phase portrait is van der Pol-like in Fig.16(a) because $|a| \ll 1$, and becomes Duffing-like in Fig.16(b) and (c). Figure 16(c) can be regarded as the saddle-connection of homoclinic orbits in the Duffing equation. The phase portraits in Fig.16(a)$\sim$(c) are symmetric but the phase

portrait in Fig.16(d) becomes asymmetric when $r = 7.4$. It is clear from Fig.16 (e)$\sim$(h) that the symmetry in the phase portrait is recovered for $7.5 \lesssim r \lesssim 7.65$. We find a *narrow-band* chaos for $r = 7.6485$ (g) and the Period-3 window for $r = 7.65$ (h) that is corresponding to Fig.18(b). Figure 18(a) corresponds to Fig.16 (e). These heteroclinic bifurcations are due to the well-known phenomenon of hysteresis. In order to explain it, we show Fig.17: the amplitude-Rayleigh number diagram with $\zeta = 0.26$, $\sigma = 1$, $w = 0.8$ and $q = 5$. In this case we have $r^{(0)} = 2.41$ from Eq.(3-9) and $q_0 = 0.7$ from Eq.(3-11). The maximum amplitudes of periodic solutions are denoted by $\bigcirc$ and those of the steady solutions are denoted by $\bullet$. The analytical steady solutions given by Eq.(6-3), which is already shown in Fig.3(d), are denoted by the dotted line in Fig.17. The branch of steady solutions has two turning points ($|a| \sim 0.5$ and 1.0) for $7.5 \lesssim r \lesssim 8.0$. There are four stable steady solutions for $r = 7.6$. Therefore a stable limit cycle coexists with the four stable steady states ($a \sim \pm 0.5$ and ± 1), and a kind of extended hysteresis can occur. Such a coexistence of multiple stable steady states and stable limit cycle gives birth to an extended hysteresis. The fixed parameters in Figs.19$\sim$23 are $\zeta = 0.1$, $\sigma = 1$, $w = 0.2353$ and $q = 5$. Figure 19 shows the time-evolution of $a(t)$ for an intermittency[34] with different r. The periodic soluton is interrupted by bursts which become more frequent as r is increased: (a)$r = 6.858$, (b)$r = 6.88$ and (c)$r = 7.2$. The time-record of oscillation of $a(t)$ in Fig.19(c) is similar to that of the density of cesium-ion in the Belousov-Zhabotinski reaction.[5] The channel corresponding to the laminar phase of intermittency[34] is clearly observed in Fig.20 at $r = 7.2$. A strange attractor projected onto the $b - c$ plane for the intermittent chaos at $r = 7.2$ is shown in Fig.21. Figure 22 is the amplitude-Rayleigh number diagram for the intermittency, where the branch of steady solutions denoted by

the dotted line. A Poincaré section projected onto the $d-d'$ plane for the intermittency is shown in Fig.23. When the aspect-ratio w is decreased, an abnormal transition to chaos from a marginally stable periodic solution is observed in Fig.24 with $\zeta = 0.1$, $\sigma = 1$, $w = 0.1081$, $q = 5$ and $r = 12.9$. This transition to chaos (Fig. 24) is different from the intermittent transition (Fig. 19) which was studied by Pomeau and Manneville [34] in the Lorenz model for the sufficiently large r. Figure 25 shows the amplitude-Rayleigh number diagram with $\zeta = 0.1$, $\sigma = 1$, $w = 0.1081\,(\lambda = 1/6)$ and $q = 5$. The branch of steady solution is already shown in Fig.2(a) which is denoted by the dotted line in Fig.25. The secondary Hopf bifurcation is clearly observed at $r \sim 12.896$ on the branch of nonlinear periodic solution in Fig. (25).

Thus our fifth-order system shows almost all the typical routes to chaos in the dissipative dynamical systems : period-doubling bifurcation, homoclinic bifurcation, heteroclinic bifurcation (an extended hysteresis), intermittency and abnormal transition to chaos. It is significant to construct a simple model whose solutions are qualitatively similar to those of the original partial differential equations. Our fifth-order system may be such a model.

9 Discussion

Since our normal form equation(7-13) has a double-zero eigenvalue, the X point in Fig.14 can be regarded as a codimension-2 point[28] ($c_1 = 0$) : X ($r_0^{(0)}$, q_0) . When $r_0^{(0)} < r$ and $q_0 \ll 1$ under the condition (4-19) with the appropriate w, for the fixed r we have the following cases (See Figs. 14 and 15) :

i. $q < q_0 + B_N\ (r - r_0^{(0)})$: steady solutions (region III),

ii. $q \sim q_0 + B_N\ (r - r_0^{(0)})$: chaos if there exists (the boundary XW),

iii. $q_0 + B_N\ (r - r_0^{(0)}) < q < \dfrac{1+\sigma}{\zeta(\sigma+\zeta)}(r - r_0^{(0)})$: periodic solutions (region II),

iv. $q > \dfrac{1+\sigma}{\zeta(\sigma+\zeta)}(r - r_0^{(0)})$: stable region I.

Let us consider a relation between the nonlinear stability boundary XW and the renormalized Holmes-Melnikov boundary given by Eq.(7-25). If we assume that this boundary (7-25) can be applied to the nonlinear stability boundary XW in Fig. 14, then it is clear that this renormalized Holmes-Melnikov boundary can be qualitatively regarded as the nonlinear stability boundary XW because

$$B_{HM} \lesssim B_N \ \sim 2.$$

Thus the renormalized Holmes-Melnikov boundary seems to be a powerful tool to look for the nonlinear stability boundary XW, where there exists a chaotic solution in certain parameter regions.

Since the perturbation[8] combined with the severely truncated Fourier series employed here is not self-consistent, pointed out by Magnan and Reiss[35] for the double-diffusive

convection, the reductive perturbation method[36] must be applied to the original partial differential equations (2-11)~(2-13) in order to obtain consistently a finite-amplitude evolution equation[37] for the two-dimensional magnetoconvection. In general Eq.(4-1) can be reduced to the Ginzburg-Landau equation[38,39] by the reducive perturbation method or the Newell-Whitehead theory,[40] which has been also derived from the case of ionization waves in the glow-discharge.[41] The Ginzburg-Landau equation shows a rich variety of spatial structure[42] and a transition to spatio-temporal chaos.[6,42] Therefore a self-consistent extension of the normal form equation to the Ginzburg-Landau type equation is fascinating topic of study.

10 Conclusion

We have studied a two-dimensional Boussinesq fluid with the nonlinear interaction between the Rayleigh-Bénard convection and an externally imposed magnetic field. We have introduced a truncated model of fifth-order system of nonlinear ordinary differential equations with five parameters and integrated it numerically in some parameter regions. Our truncated model is a straightforward extension of the Lorenz model taken account the Lorentz force. We found various types of bifurcations from periodic solutions : homoclinic bifurcation, period-doubling bifurcation, heteroclinic bifurcation (extended hysteresis), intermittent chaos and abnormal transition to chaos, which differ significantly from some of previously reported results. [8~13,26,27] We have also derived a normal form equation from our fifth-order system, applying the center manifold theory to it, and given an expression for the Holmes-Melnikov boundary to evaluate numerical results. By means of the normal form equation, we have shown that each property of the two phase portraits described by the Duffing equation and the van der Pol equation emanates from one common attractor in the five-dimensional space.

Let us list the principal results of this investigation :

1. the simple bifurcation at $r = r^{(e)}$ is supercritical in the absence of magnetic field ($q = 0$) (See Fig. 1 (a)) ;

2. the simple bifurcation at $r = r^{(e)}$ is not always supercritical in the presence of magnetic field ($q \neq 0$) (See Fig. 1 (b)~(g)) ;

3. the branch of steady solution at $r = r^{(e)}$ becomes unstable drastically due to the appearance of periodic solution (limit cycle) (See Fig. 8) ;

4. the sign of $r_2^{(e)}$ has an significant effect on the steady solution in double-diffusive systems, [8~11,13,26,27] but it does not always determine whether the branch of steady solution is supercritical or subcritical (See Figs. 1~6) ;

5. the branch of periodic solution bifurcates supercritically from the static solution at $r = r^{(e)}$, corresponding to the linear boundary XV in the stability diagram (See Fig. 14) ;

6. the amplitude of periodic solution becomes large as r is increased (See Fig. 8) ;

7. the behaviours of periodic solutions with finite-amplitude can be qualitatively explained by the normal form equation (7-13) since these periodic solutions (7-13) obtained analytically at small amplitude persist to larger amplitudes in some parameter regions ;

8. the branch of chaotic solution in certain parameter regions bifurcates supercritically from the finite-amplitude periodic solution, not from the steady solution, while in sufficiently large r bifurcates subcritically from the steady solution (the subcritical Hopf bifurcation in the Lorenz type system, See Fig. 7) ;

9. the branch of chaotic solution may be regarded as the secondary Hopf bifurcation in some parameter regions ;

10. there are various types of chaotic solutions with different parameters;
    (i). period-doubling bifurcation (See Fig. 9),
    (ii). heteroclinic bifurcation (See Fig. 16),
    (iii). intermittent chaos (See Fig. 21),

(iv). abnormal transition to chaos (See Fig. 24) ;

11. the value corresponding to the Feigenbaum constant[43] is approximately given by $\delta_1 \sim 4 \pm 1.0$ in terms of Period-2, Period-4 and Period-8 (See Fig. 9) ;

12. routes to chaos are not always through the period-doubling cascade ;

13. the numerical results of Eq.(5-2) are qualitatively agreement with those of the original partial differential equations $(2-11) \sim (2-13)$ obtained by Weiss[14] except for the chaotic solutions ;

14. each property of the two phase portraits described by the Duffing equation and the van der Pol equation emanates from one common attractor in the five-dimensional space ;

15. the renormalized Holmes-Melnikov boundary (7-25) can explain qualitatively the nonliear stability boundary XW obtained numerically, where there exists a chaotic solution in certain parameter regions.

Since there are the five fundamental parameters in our system, we must construct a theory to contain the higher codimension. The theory of bifurcations of higher codimension may be casting light on the understanding of more general magnetoconvection. Although there exists a limit that our fifth-order system is no longer a valid approximation to the original partial differential equations in some parameter regions, our truncated model may serve as *a paradigm* for all the turbulence related to the Lorentz force.

Acknowledgements

One of the authors (N.B.) is indebted to Professor T. Tajima for bringing to his attention the problem of magnetoconvection. We are grateful to Kazuhiro Nozaki and Ippei Shimada for their helpful discussions. This work was partly performed as the collaborating program at National Institute for Fusion Science.

References

[1] N.J. Zabusky and M.D. Kruskal: Phys. Rev. Lett. **15**, 240 (1965).

[2] E.N. Lorenz : J. Atmos. Sci. **20**, 130 (1963).

[3] E. Fermi, J. Pasta and S. Ulam : *Los Alamos Report*, LA 1940 (1955).

[4] N. Saito and H. Hirooka : J. Phys. Soc. Jpn. **23**, 167 (1967).

[5] P. Bergé, Y. Pomeau and C. Vidal : *Order within Chaos*, Johon Wiley & Sons (1984).

[6] K. Nozaki and N. Bekki : Phys. Rev. Lett. **51**, 2171 (1983).

[7] K. Nozaki and N. Bekki : Physica D,**21D**, 381 (1986).

[8] E. Knobloch and M.R.E. Proctor : J.Fluid Mech.**108**, 291(1981).

[9] E. Knobloch,N.O. Weiss and L.N. da Costa : J. Fluid Mech. **113**, 153 (1981).

[10] L.N. da Costa, E.Knobloch and N.O.Weiss : J. Fluid Mech. **109**, 25 (1981).

[11] E. Knobloch and N.O. Weiss : Physica D, **9D**,379 (1983).

[12] E.Knobloch, D.R.Moore, J.Toomre and N.O.Weiss : J. Fluid Mech. **166**, 409 (1986).

[13] M.R.E. Proctor and N.O. Weiss : Rep. Prog. Phys. **45**, 1317 (1982).

[14] N.O. Weiss : J. Fluid Mech.**108**, 247(1981), J. Fluid Mech. **108**, 273 (1981).

[15] V. Franceschini and C. Tebaldi : J. Stat. Phys. **21**, 707 (1979).

[16] N. Nakajima : Phys. Fluids **B2**,1170(1990).

[17] N. Bekki and Y. Kaneda : Phys. Rev. Lett. **57**, 2176 (1986).

[18] S. Hamaguchi : Phys. Fluids **B1**,1416 (1989).

[19] W. Horton, B.G. Hong, T. Tajima and N. Bekki : Comments Plasma Phys. Controlled Fusion **13**,207 (1990).

[20] F.H. Busse : J. Fluid Mech.**71**, 193(1975).

[21] S. Chandrasekhar : Phil. Mag.**43**, 501 (1952), *Hydrodynamic and Hydromagnetic Stability* , Oxford:Clarendon (1961).

[22] E.N. Parker : *Cosmical Magnetic Fields*, Oxford:Clarendon (1979).

[23] G. Veronis : J. Fluid Mech. **5**, 401 (1959).

[24] G. Veronis : J. Fluid Mech. **4**, 545 (1966).

[25] C. Sparrow : *The Lorenz Equations*, Springer-Verlag (1982).

[26] A.M. Rucklidge : J. Fluid Mech. **237**, 209 (1992).

[27] E. Knobloch, M.R.E. Proctor and N.O. Weiss : J. Fluid Mech. **239**, 273 (1992).

[28] J. Guckenheimer and P. Holmes : *Nonlinear Oscillations, Dynamical Systems, and Bifurcations of Vector Fields*, 2nd Edition, Springer-Verlag (1986).

[29] F. Takens : Publ. Math. IHES, **43**, 47 (1974).

[30] R.I. Bogdanov : Functional Analysis and Its Applications, **9** (2), 144 (1975).

[31] S. Smale : Bull. Amer. Math. Soc. **73**, 734 (1967).

[32] P.J. Holmes : Phil. Trans. Roy. Soc. A**292**, 419 (1979).

[33] Y. Ueda : J. Stat. Phys. **20**, 181 (1979).

[34] Y. Pomeau and P. Manneville : Commun. Math. Phiys. **74**, 189 (1980).

[35] J.F. Magnan and E.L. Reiss : Phys. Rev. A,**31**, 1841 (1985).

[36] T. Taniuti : Suppl. of Prog. Theor. Phys. **55**, 1(1974).

[37] A.C. Newell, T. Passot and J. Lega : Annu. Rev. Fluid Mech. **25**, 399 (1993).

[38] K. Stewartson and J.T. Stuart : J. Fluid Mech. **48**, 529 (1971).

[39] Y. Kuramoto and T. Tsuzuki : Prog. Theor. Phys. **55**, 356 (1976).

[40] A.C. Newell and J.A. Whitehead : J. Fluid Mech. **38**, 279 (1969).

[41] N. Bekki : J. Phys. Soc. Jpn. **50**, 659 (1981).

[42] I. Aranson, H. Levine and L. Tsimring : Phys. Rev. Lett. **72**, 2561 (1994).

[43] M.J. Feigenbaum : J. Stat. Phys. **19**, 25 (1978).

Figure Captions

1. The amplitude-Rayleigh number diagram of steady solutions of the velocity $|a|$ for the different q with the fixed $\zeta = 0.1$ and $w = 0.8$; (a) $q = 0$, (b) $q = 1$, (c) $q = 2$, (d) $q = 3$, (e) $q = 5$, (f) $q = 10$ and (g) $q = 15$.

2. The amplitude-Rayleigh number diagram of steady solutions of the velocity $|a|$ for the different w with the fixed $\zeta = 0.1$ and $q = 5$; $(a)w = 0.1081(\lambda = 1/6)$, $(b)w = 0.2353(\lambda = 1/4)$, $(c)w = 0.8(\lambda = 1/2)$, $(d)w = 2.0(\lambda = 1)$, $(e)w = 3.2(\lambda = 2)$, $(f)w = 3.6(\lambda = 3)$ and $(g)w = 0.37647(\lambda = 4)$.

3. The amplitude-Rayleigh number diagram of steady solutions of the velocity $|a|$ for the different ζ with the fixed $w = 0.8$ and $q = 5$; $(a)\zeta = 0.01$, $(b)\zeta = 0.1$, $(c)\zeta = 0.2$, $(d)\zeta = 0.26$, $(e)\zeta = 0.3$, $(f)\zeta = 0.4$ and $(g)\zeta = 0.5$.

4. The amplitude-Rayleigh number diagram of steady solutions of the velocity $|a|$ for the different ζ with the fixed $w = 2$ and $q = 5$; $(a)\zeta = 0.01$, $(b)\zeta = 0.1$, $(c)\zeta = 0.26$, $(d)\zeta = 0.3$, $(e)\zeta = 0.4$, $(f)\zeta = 0.6$ and $(g)\zeta = 0.9$.

5. The amplitude-Rayleigh number diagram of steady solutions of the velocity $|a|$ for the different ζ with the fixed $w = 3.2$ and $q = 5$; $(a)\zeta = 0.01$, $(b)\zeta = 0.1$, $(c)\zeta = 0.2$, $(d)\zeta = 0.26$, $(e)\zeta = 0.3$, $(f)\zeta = 0.4$ and $(g)\zeta = 0.5$.

6. The amplitude-Rayleigh number diagram of steady solutions of the velocity $|a|$ for the different ζ with the fixed $w = 3.6$ and $q = 5$; $(a)\zeta = 0.01$, $(b)\zeta = 0.1$, $(c)\zeta = 0.2$, $(d)\zeta = 0.26$, $(e)\zeta = 0.3$, $(f)\zeta = 0.4$ and $(g)\zeta = 0.5$.

7. (a) A Lorenz type strange attractor projected onto the $b - c$ plane.

(b) A Poincaré return-map of the successive maxima of $c(t)$ in the presence of magnetic field ($q = 5$).

(c) A Poincaré return-map of the successive maxima of $c(t)$ without magnetic field ($q = 0$) . All the parameters used here are $\sigma = 10$, $\zeta = 0.5$, $w = 2$ and $r = 30$.

8. The amplitude-Rayleigh number diagram with $\zeta = 0.1$, $\sigma = 1$, $w = 0.8$ and $q = 5$, $|a|$ means the maximum amplitude of $a(t)$ for the branch of periodic and chaotic solutions (denoted by ○ and ▲) and does the absolute value of a for the branch of steady solutions (denoted by ●). Unstable steady solutions are indicated by the dotted line.

9. A sequence of period-doubling bifurcations. Return-maps for the fixed parameters ($\zeta = 0.1$, $\sigma = 1$, $w = 0.8$ and $q = 5$) are shown when r is increased : (a) Period-2 at $r = 3.417$, (b) Period-4 at $r = 3.421$, (c) Period-8 at $r = 3.4218$, (d) Period-finite at $r = 3.422$, (e) Chaos at $r = 3.425$, (f) Chaos at $r = 3.43$, (g) Period-5 window at $r = 3.437$, (h) Chaos at $r = 3.44$, (i) Period-5 window at $r = 3.445$, (j) Chaos at $r = 3.446$.

10. Phase portraits projected onto the $a - a'$ and $d - d'$ planes from one common attractor. (a) Chaos at $r = 3.44$ which corresponds to Fig. 9 (h), (b) Period-5 window at $r = 3.4375$ which corresponds to Fig. 9 (g).

11. A set of time-evolution of chaotic solutions , corresponding to Fig. 10(a).

12. A strange attractor projected onto the $b - c$ plane, corresponding to Fig. 10(a). It is clear that this attractor is different from Fig. 7(a) (the Lorenz type attractor).

13. A Poincaré section of magnetic flux $d(t)$ projected onto the $d-d'$ plane, corresponding to Fig 10(a).

14. The stability diagram for the Chandrasekhar number versus the Rayleigh number with $\zeta = 0.1$, $\sigma = 1$ and $w = 0.8$. L_1, L_2 and L_3 are corresponding to Fig.15 (a), Fig.15 (b) and Fig.8, respectively.

15. The amplitude-Chandrasekhar number diagram with $\zeta = 0.1$, $\sigma = 1$ and $w = 0.8$: (a) $r = 3.44$ (L_1), (b) $r = 2$ (L_2).

16. A sequence of heteroclinic bifurcations : phase portraits projected onto the $a - a'$ plane ($-3 \leq a \leq 3, -3 \leq a' \leq 3$) with $\zeta = 0.26$, $\sigma = 1$, $w = 0.8$ and $q = 5$ when r is increased. (a) $r = 3$, (b) $r = 6$, (c) $r = 7.3$, (d) $r = 7.4$, (e) $r = 7.5$, (f) $r = 7.6$, (g) a $narrow - band$ chaos at $r = 7.6485$, (h) Period-3 window at $r = 7.65$.

17. The amplitude-Rayleigh number diagram with $\zeta = 0.26$, $\sigma = 1$, $w = 0.8$ and $q = 5$.

18. Time-evolution of $a(t)$ for an extended hysteresis :

    (a) heteroclinic bifurcation at $r = 7.5$, corresponding to Fig.16 (e),

    (b) Period-3 window at $r = 7.65$, corresponding to Fig.16 (h).

19. Time-evolution of $a(t)$ for an intermittency with $\zeta = 0.1$, $\sigma = 1$, $w = 0.2353$ and $q = 5$. The oscillations are interrupted by bursts which become more frequent as r is increased. (a) $r = 6.858$, (b) $r = 6.88$ and (c) $r = 7.2$.

20. A part of the return-map of the successive maxima of $a(t)$ for $r = 7.2$ during the 5×10^5 iterations, corresponding to Fig. 19 (c).

21. A strange attractor projected onto the $b - c$ plane for the intermittent chaos with $r = 6.858$.

22. The amplitude-Rayleigh number diagram for the intermittency with $\zeta = 0.1$, $\sigma = 1$, $q = 5$ and $w = 0.2353$.

23. A Poincaré section projected onto the $d - d'$ plane with $\zeta = 0.1$, $\sigma = 1$, $w = 0.2353$, $q = 5$ and $r = 6.858$.

24. Time-evolution of $a(t)$ with $\zeta = 0.1$, $\sigma = 1$, $w = 0.1081$, $q = 5$ and $r = 12.9$.

25. The amplitude-Rayleigh number diagram with $\zeta = 0.1$, $\sigma = 1$, $w = 0.1081$ and $q = 5$. Periodic solutions are denoted by ○, chaos by ▲ and steady solutions by ●.

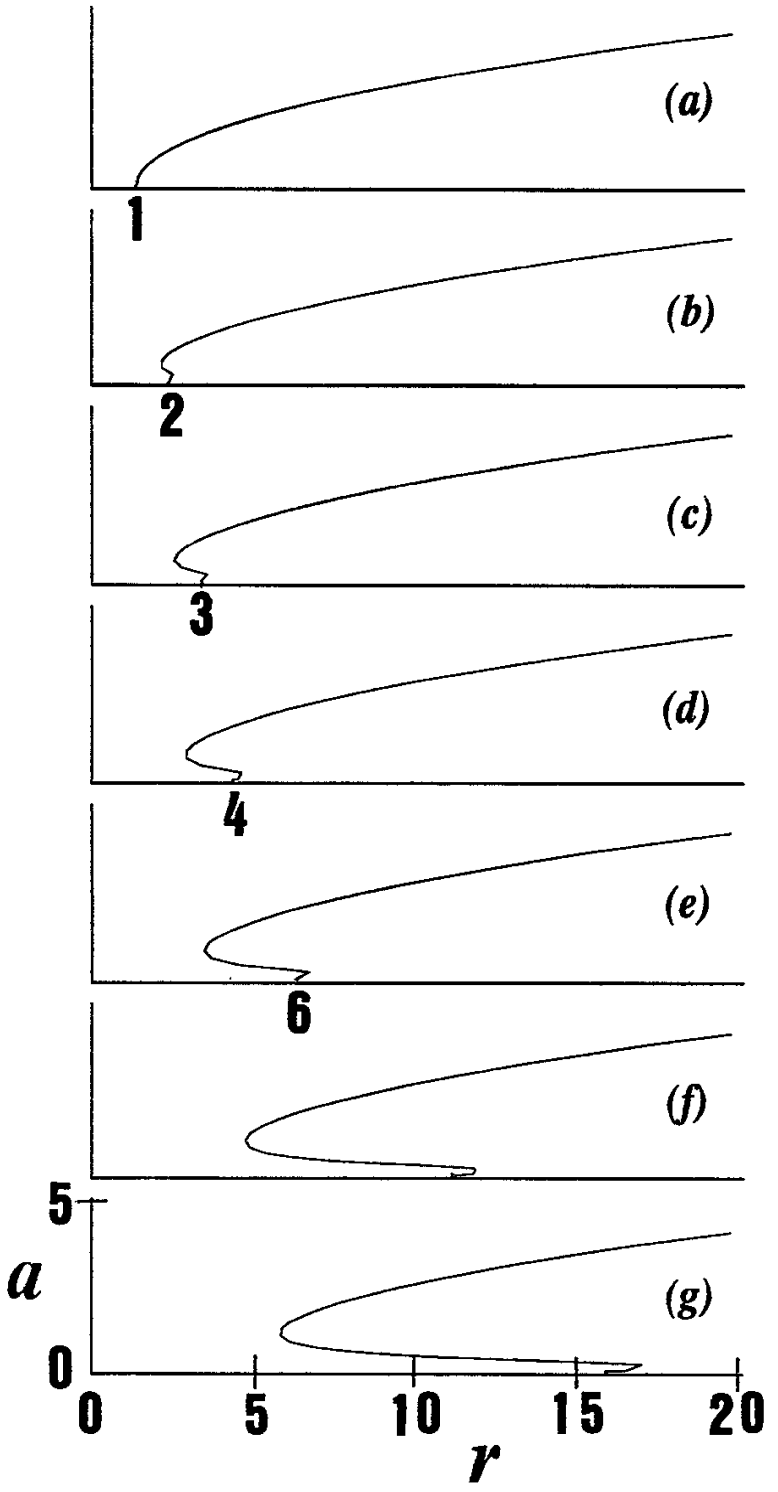

Fig . 1

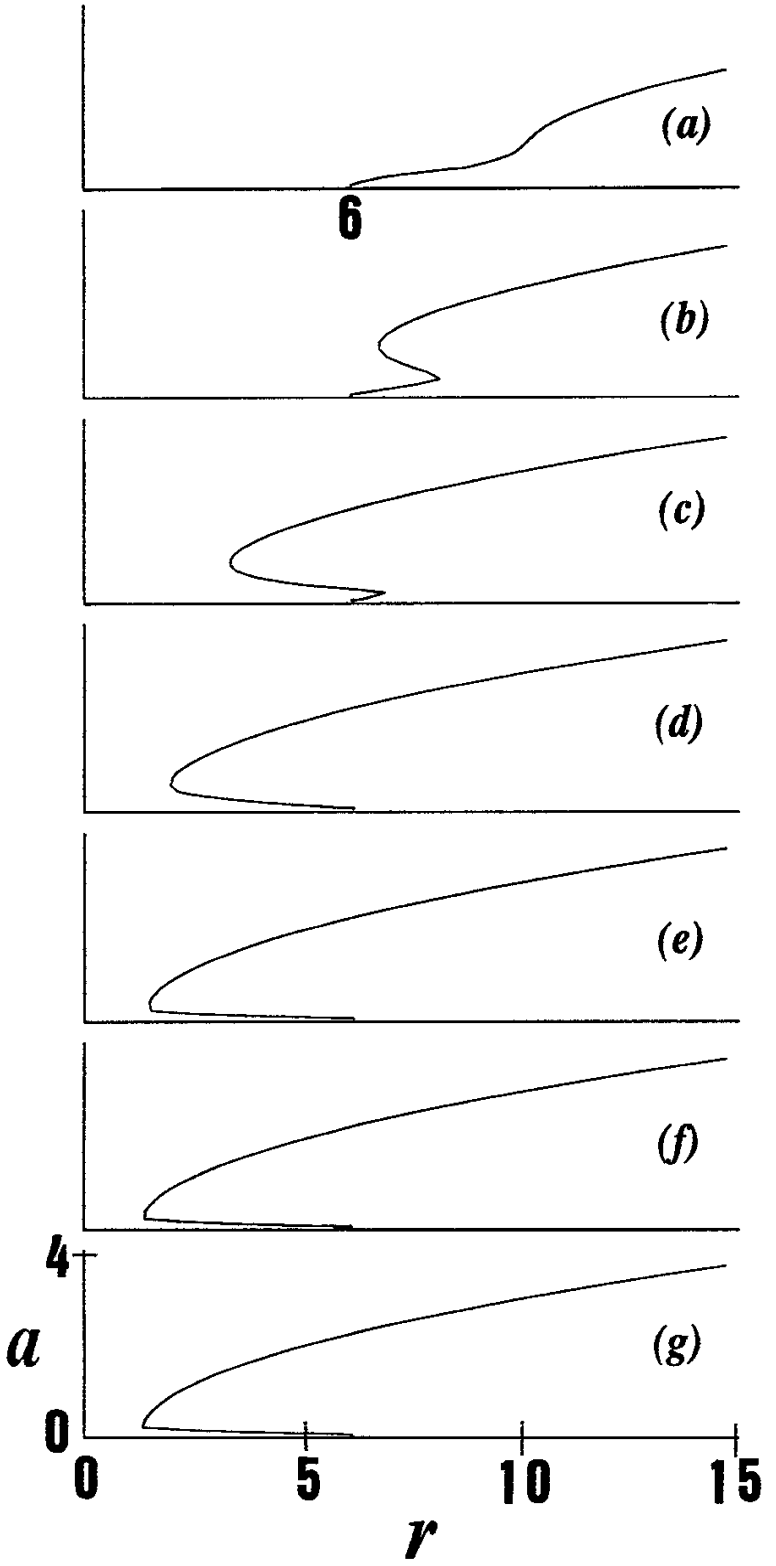

Fig . 2

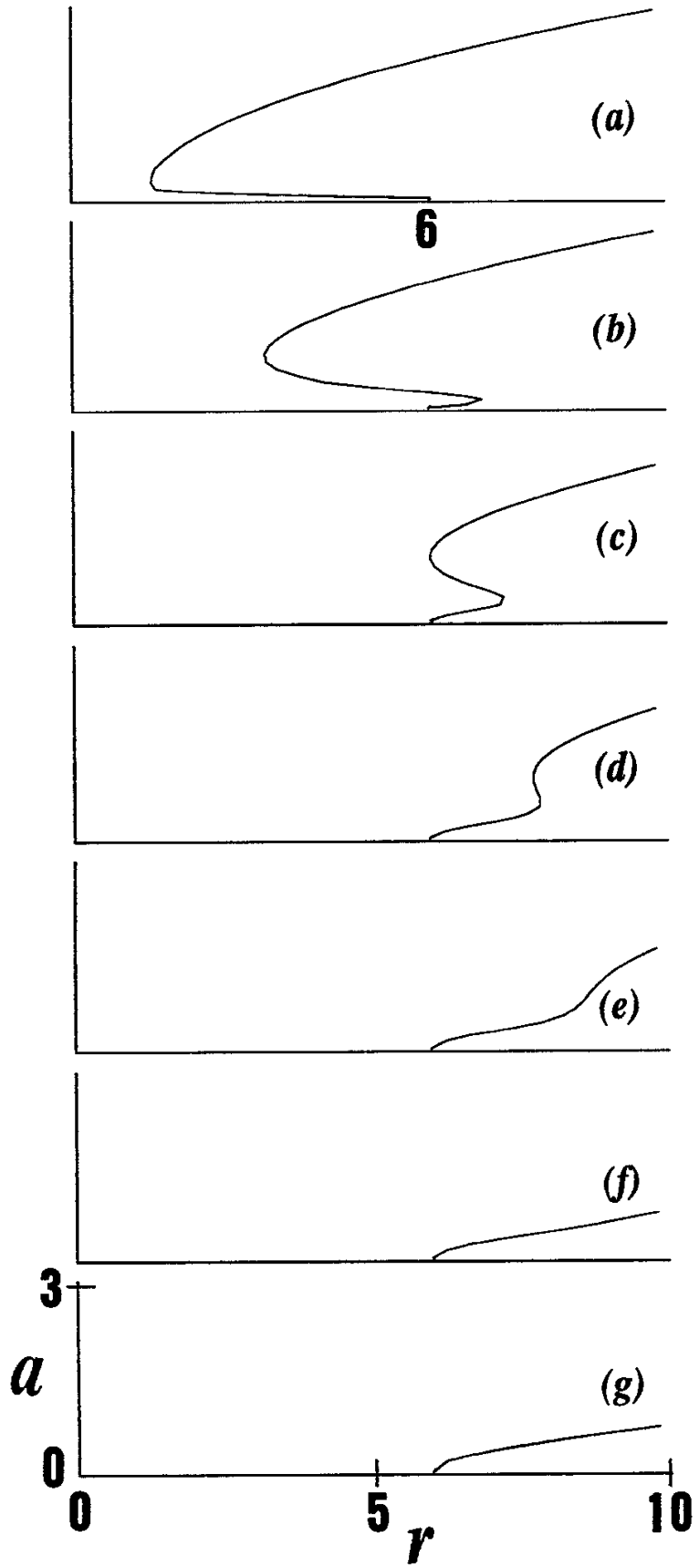

Fig . 3

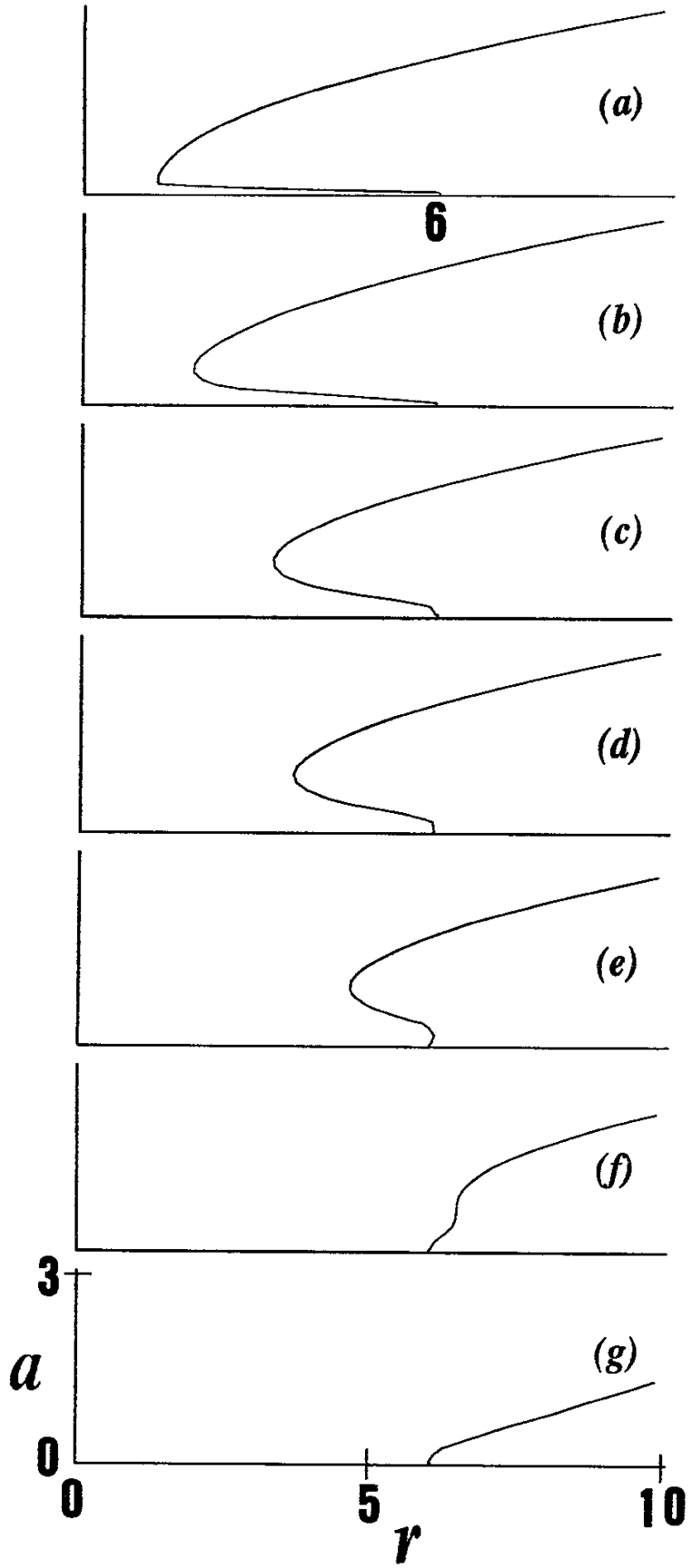

Fig . 4

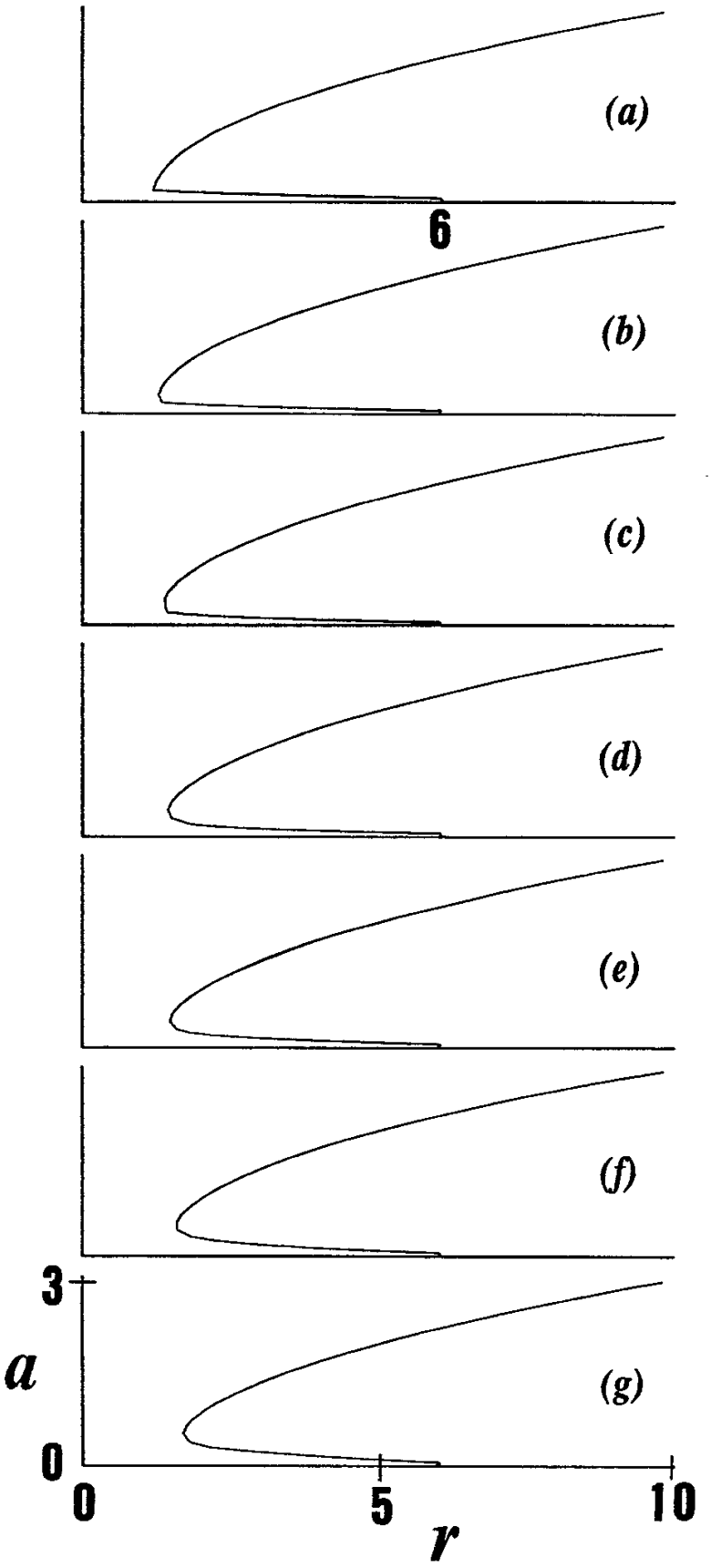

Fig . 5

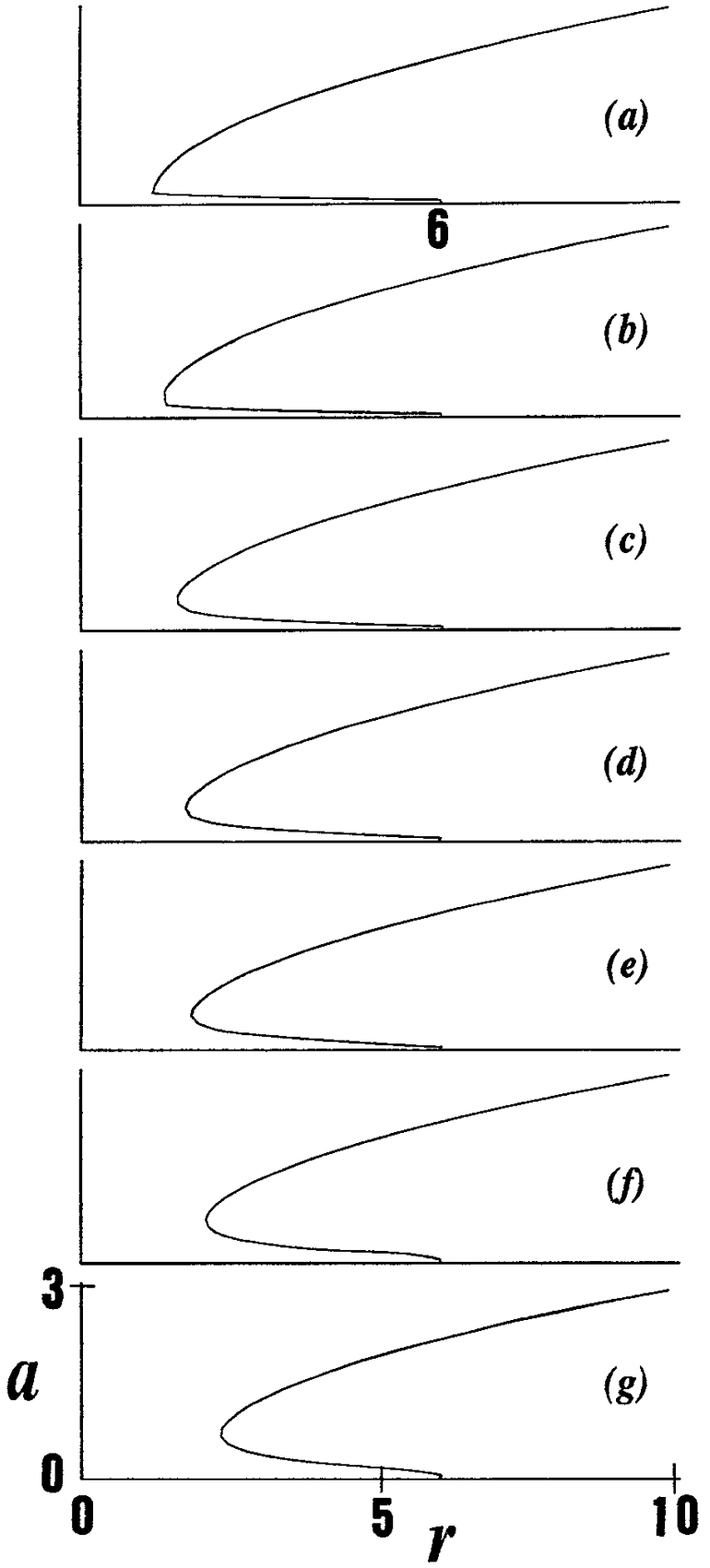

Fig . 6

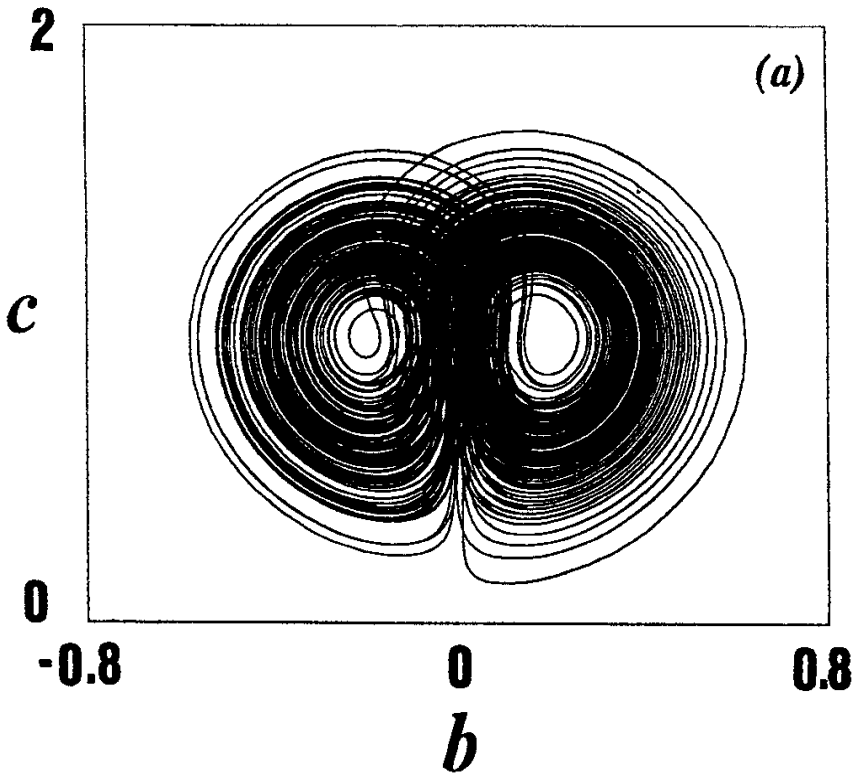

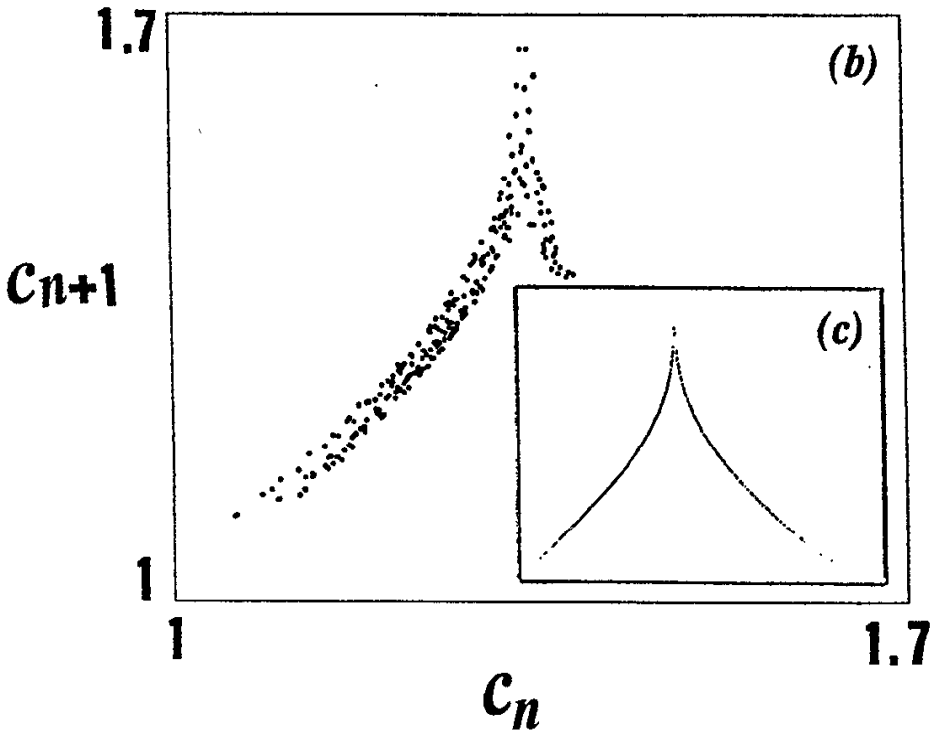

Fig . 7

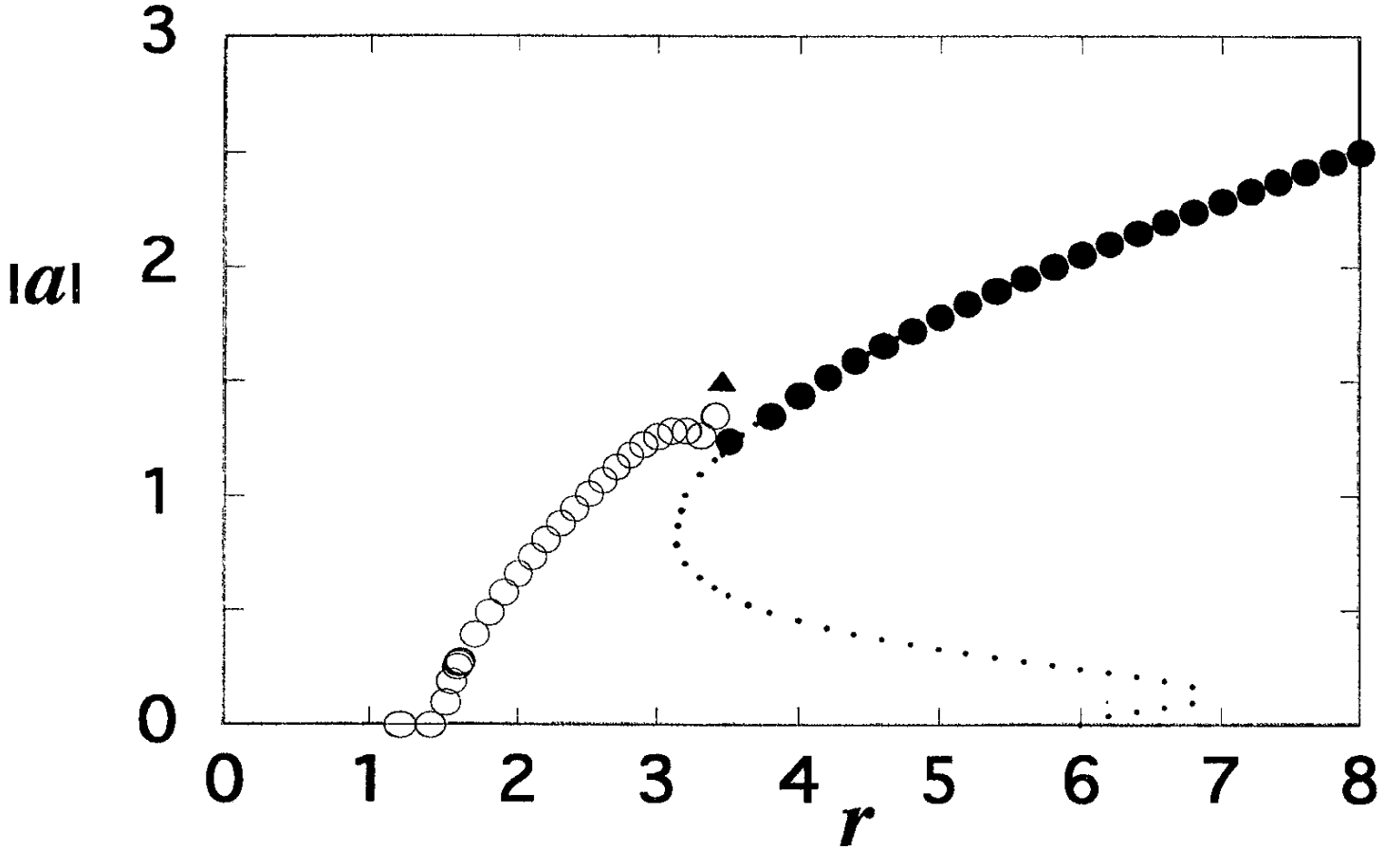

Fig . 8

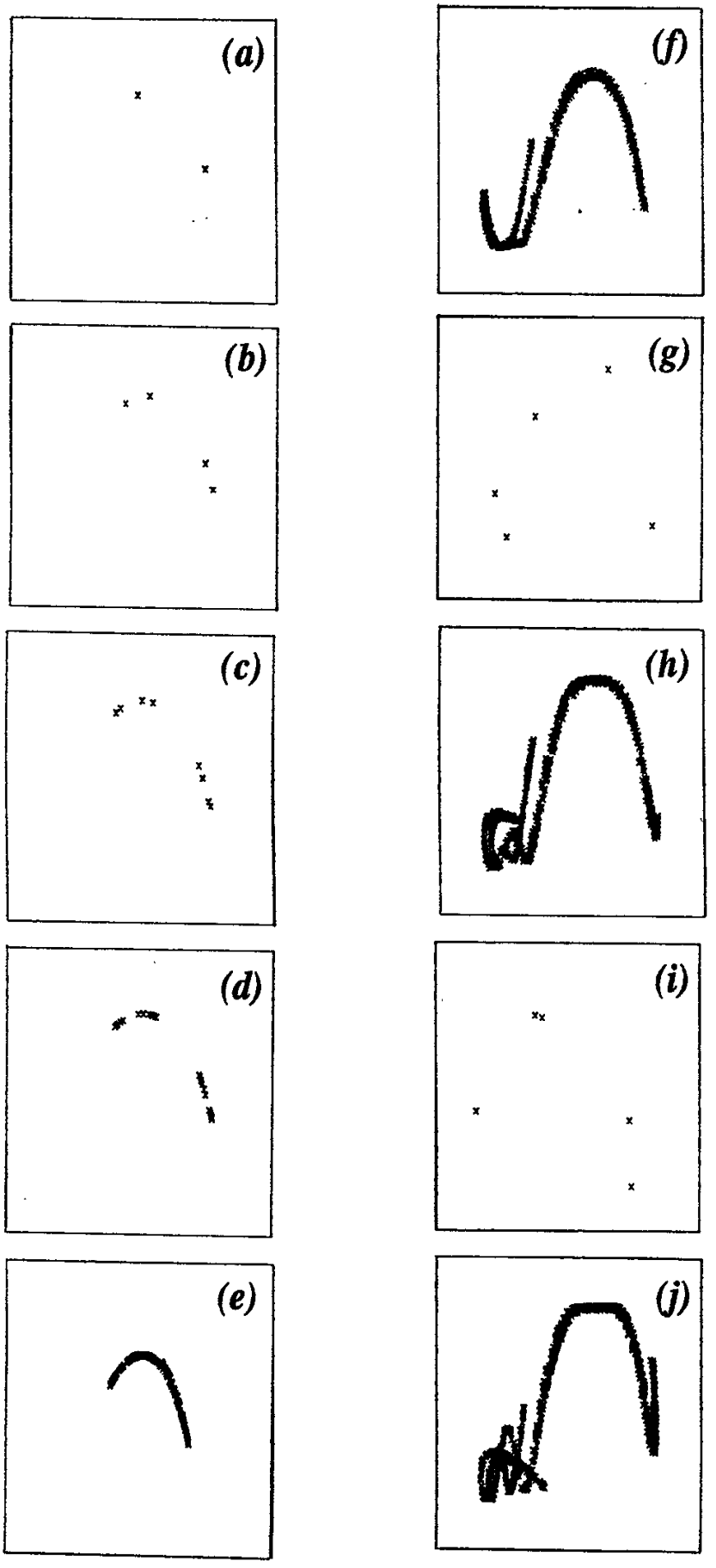

Fig . 9

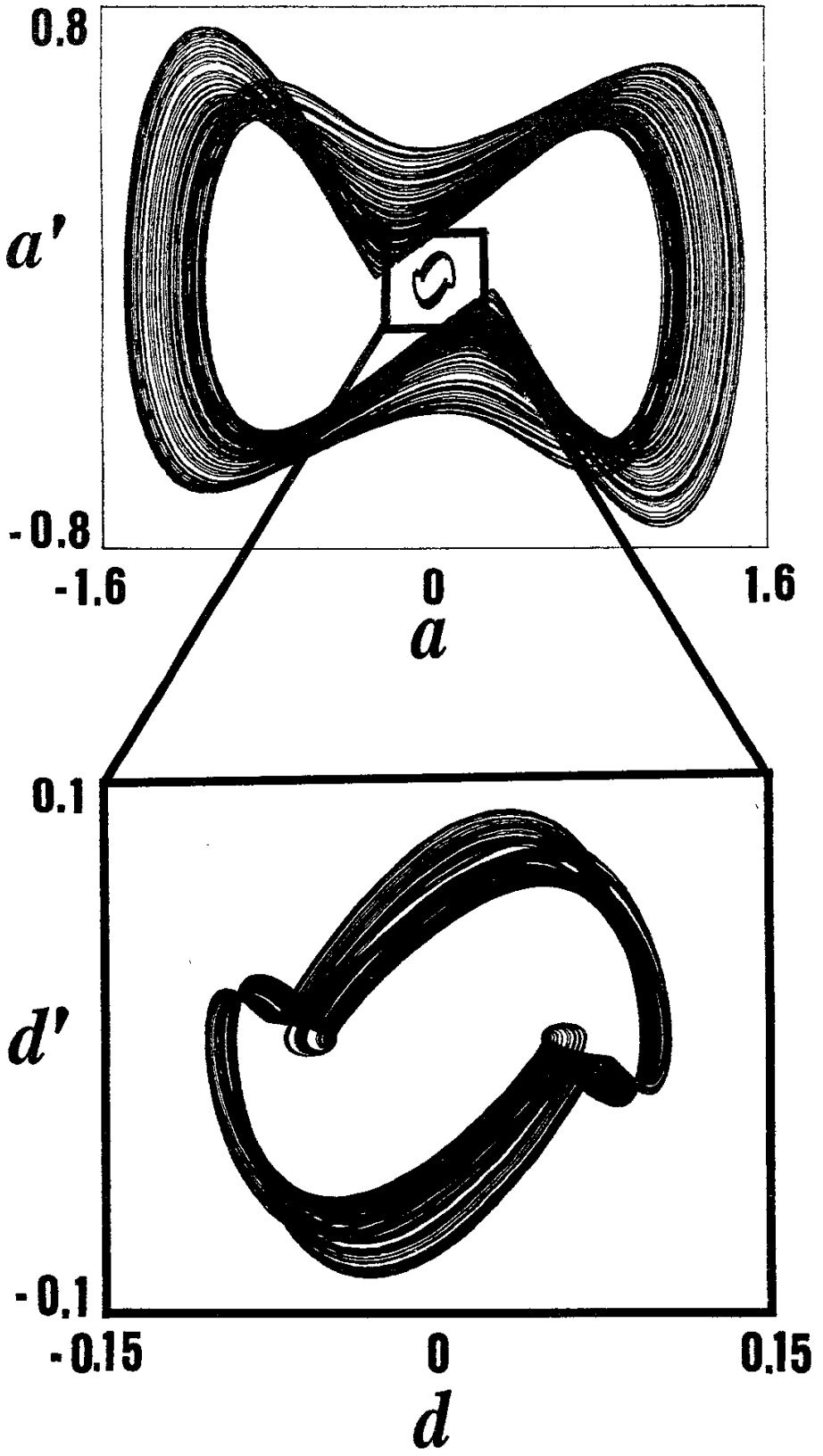

Fig . 10 (a)

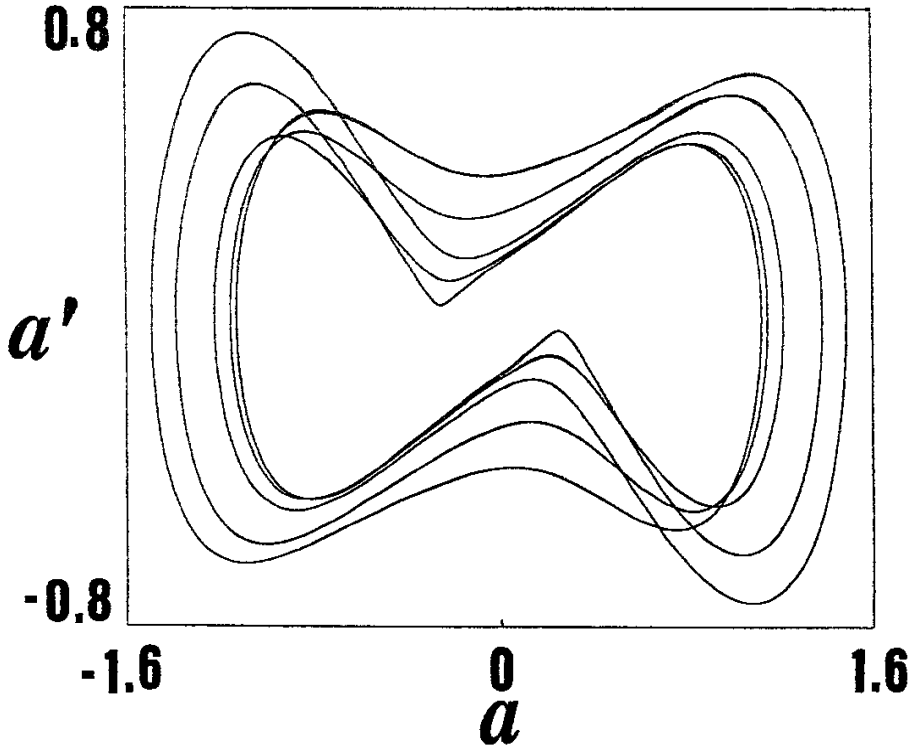

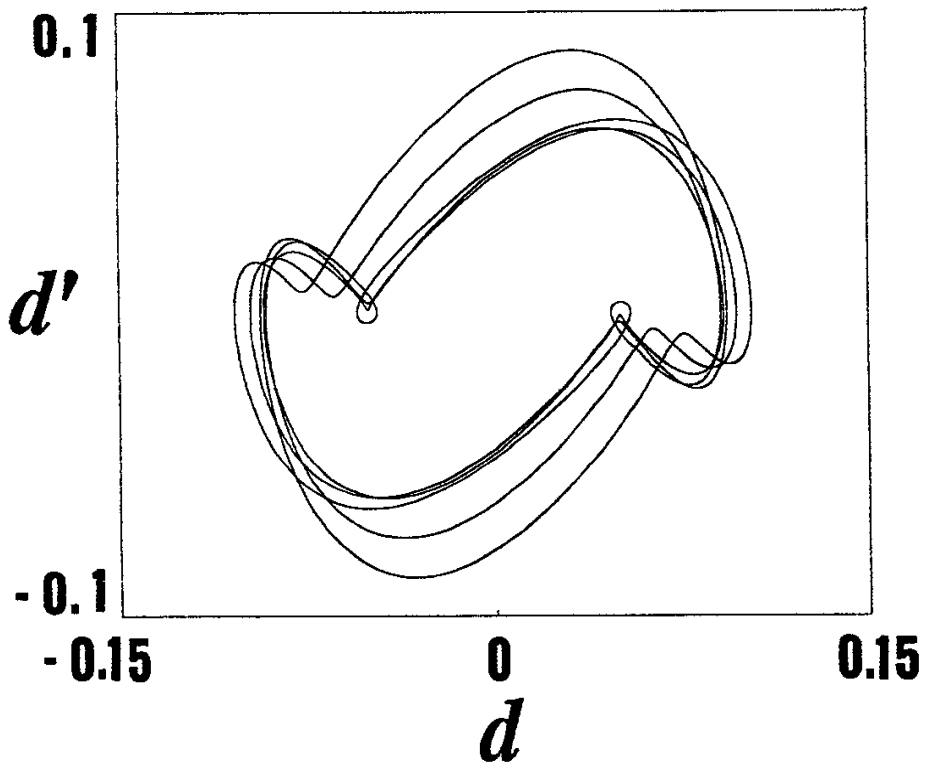

Fig . 10(b)

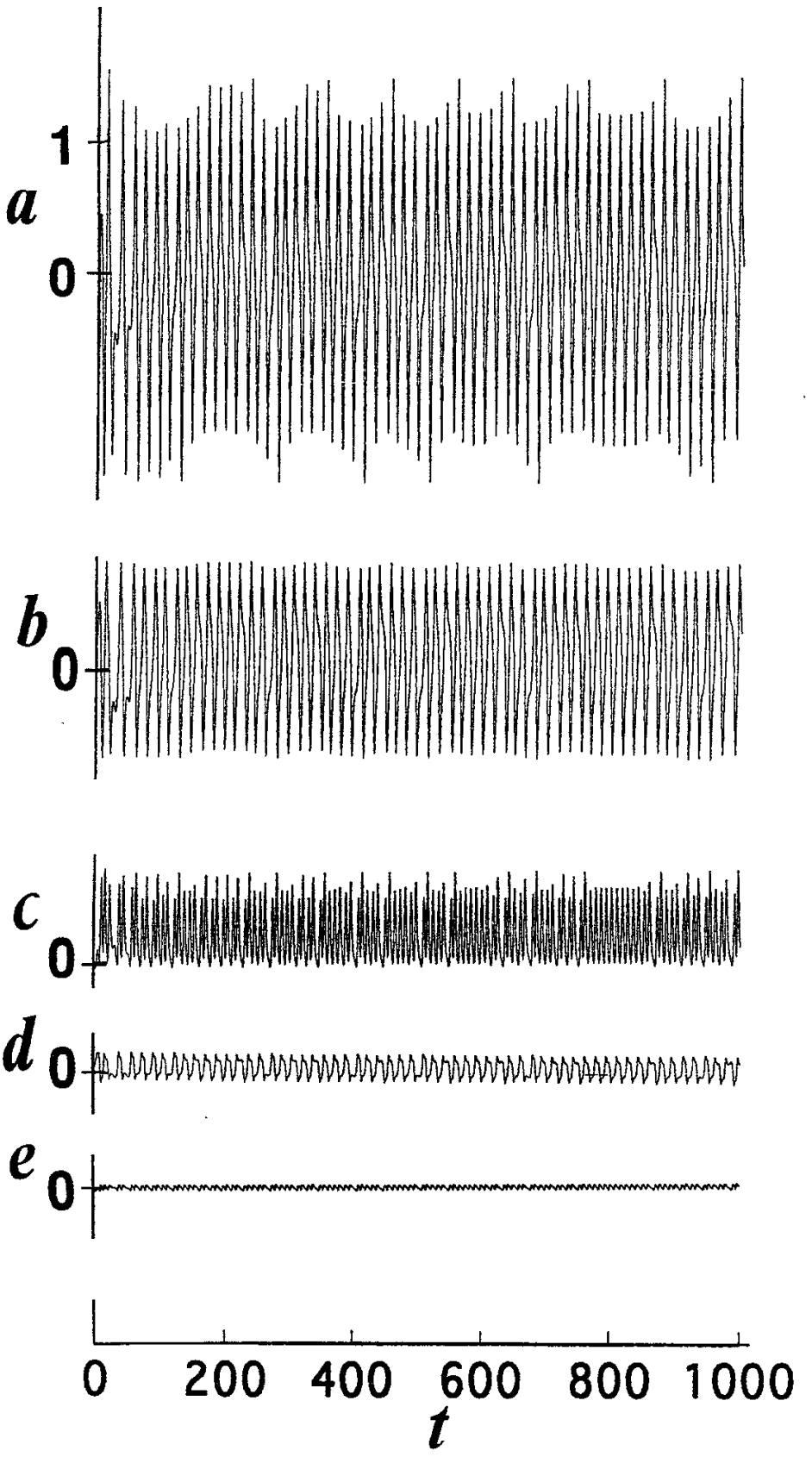

Fig . 11

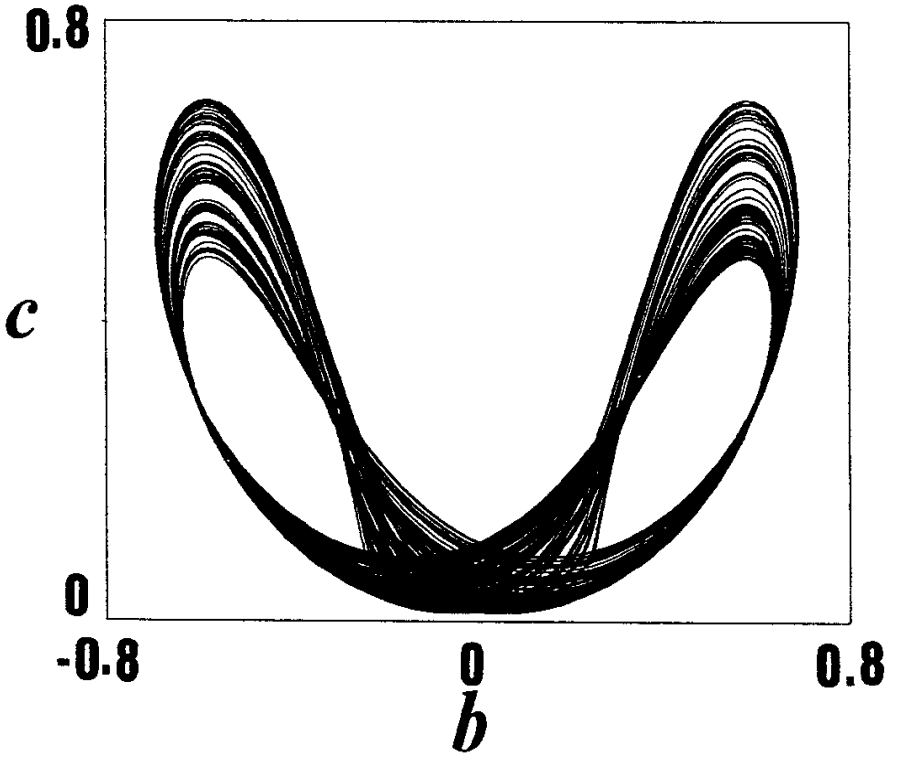

Fig . 1 2

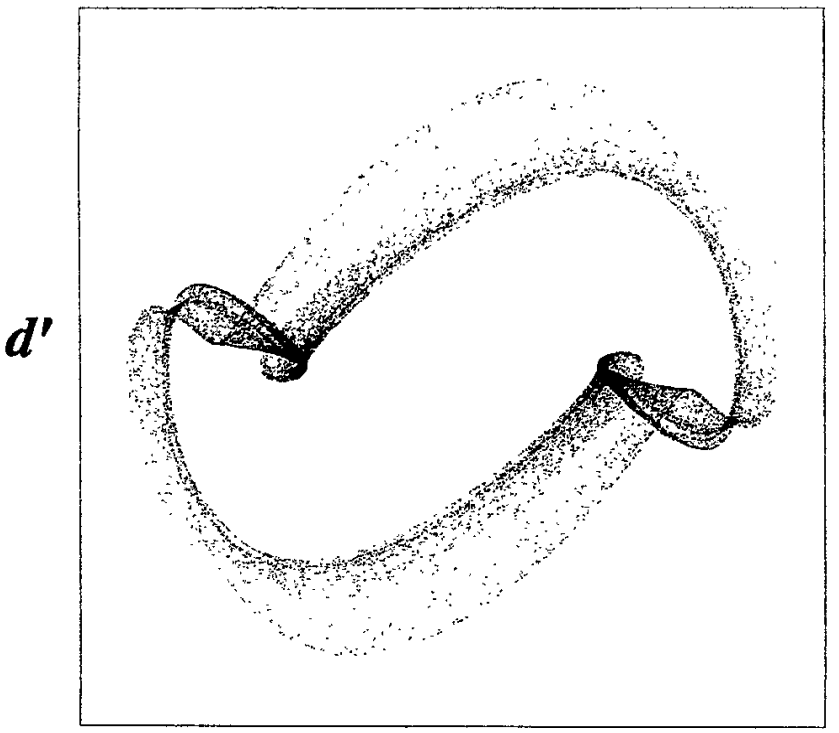

Fig . 13

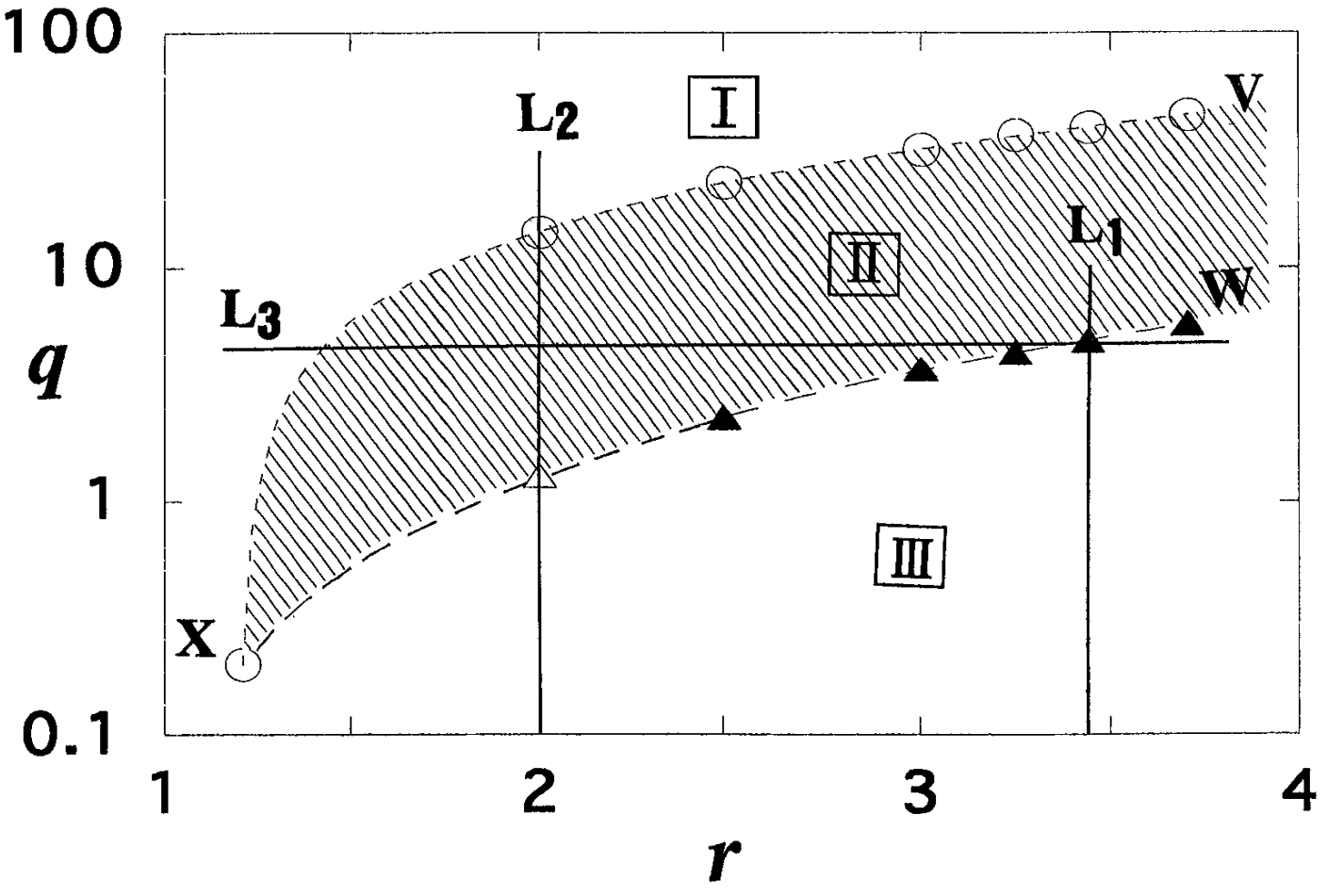

Fig . 14

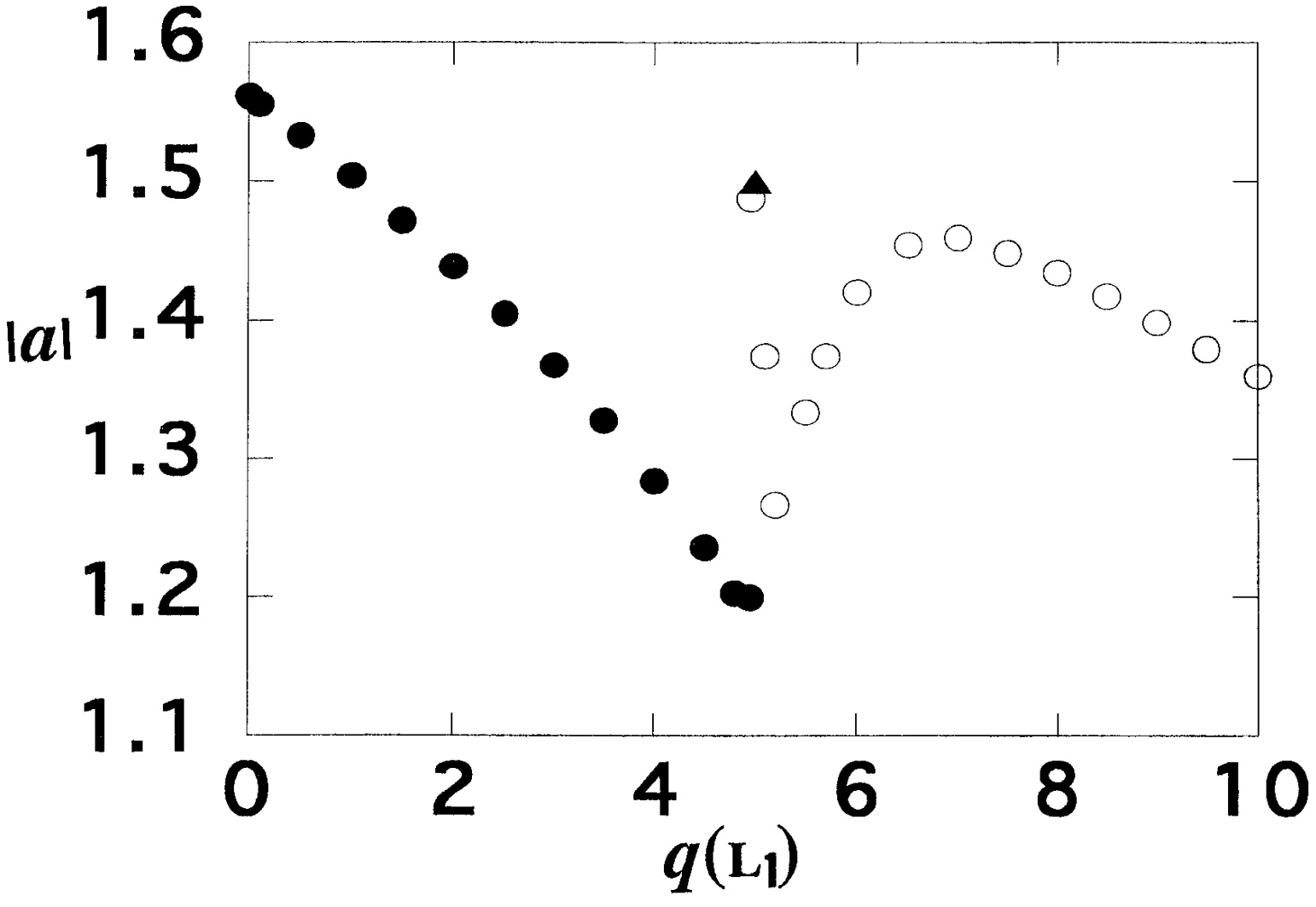

Fig . 15(a)

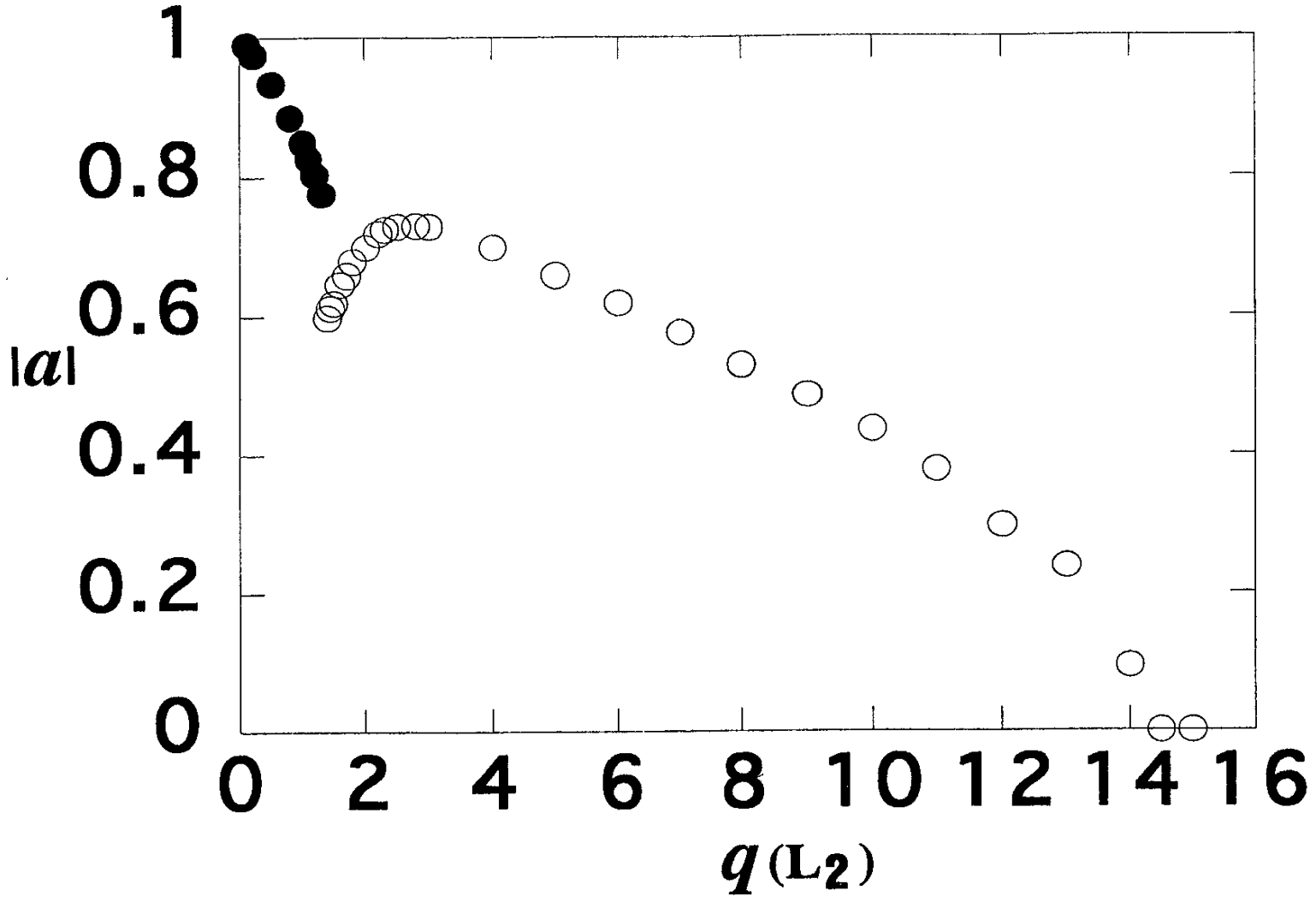

Fig . 15(b)

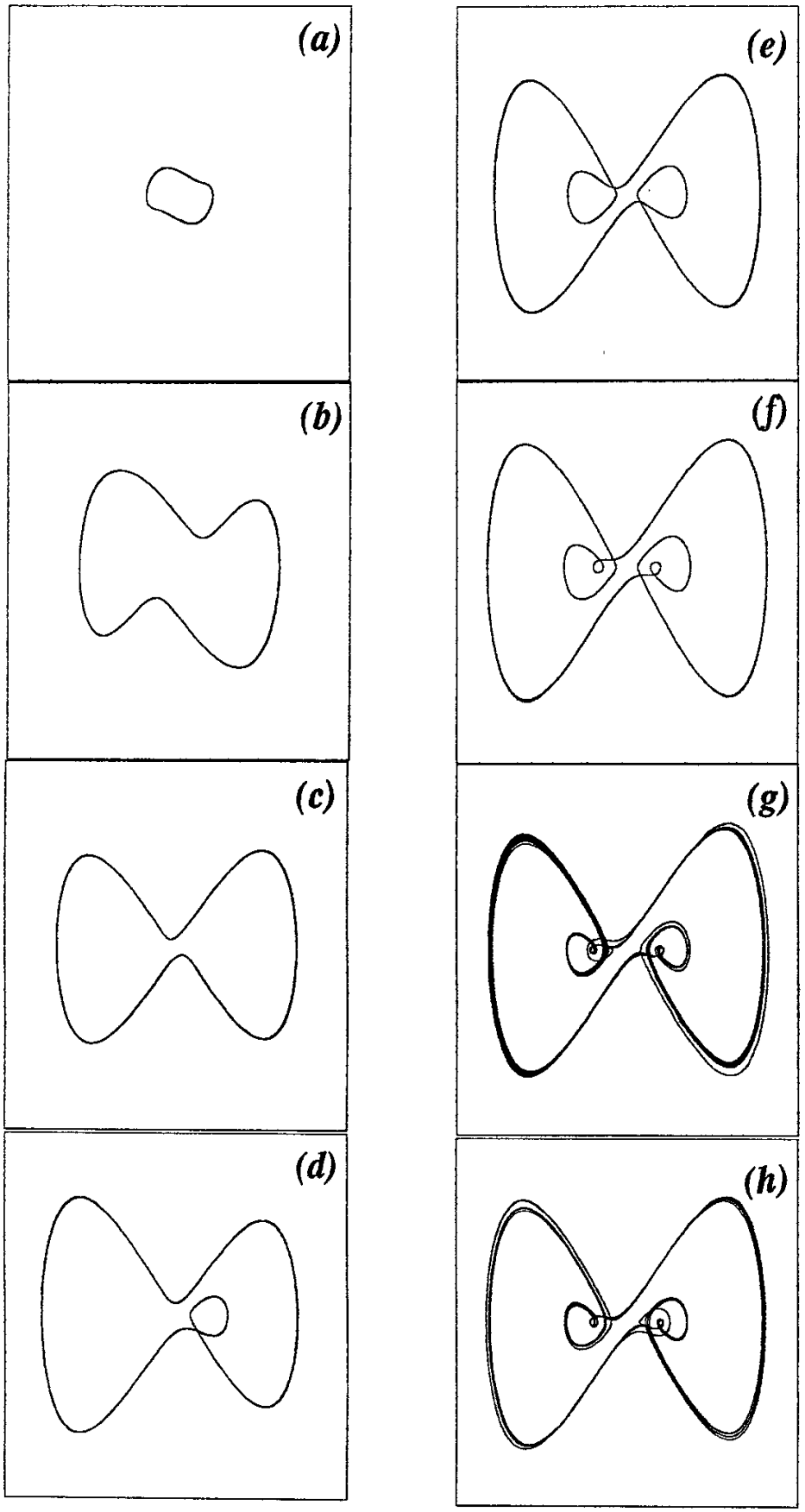

Fig .16

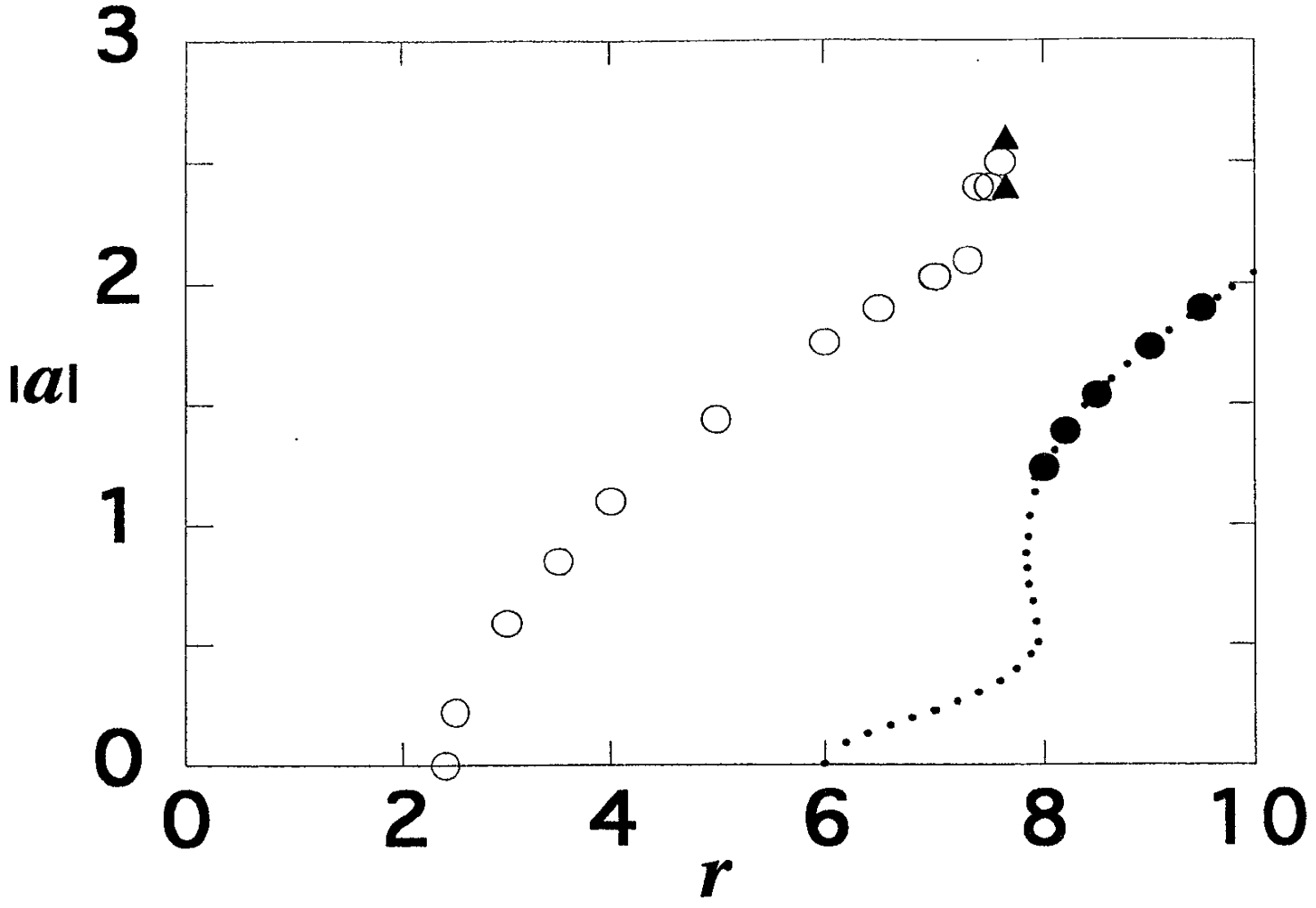

Fig .17

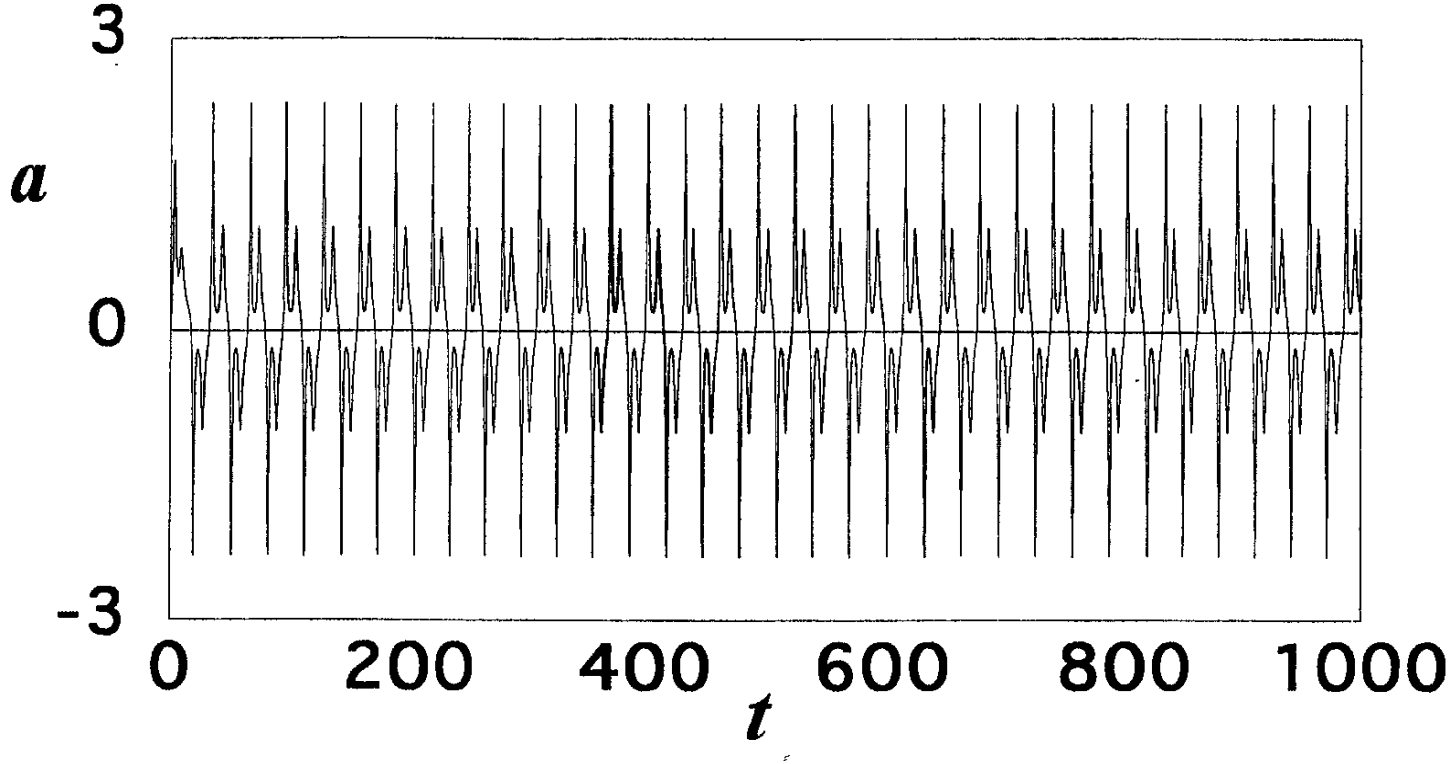

Fig . 18(a)

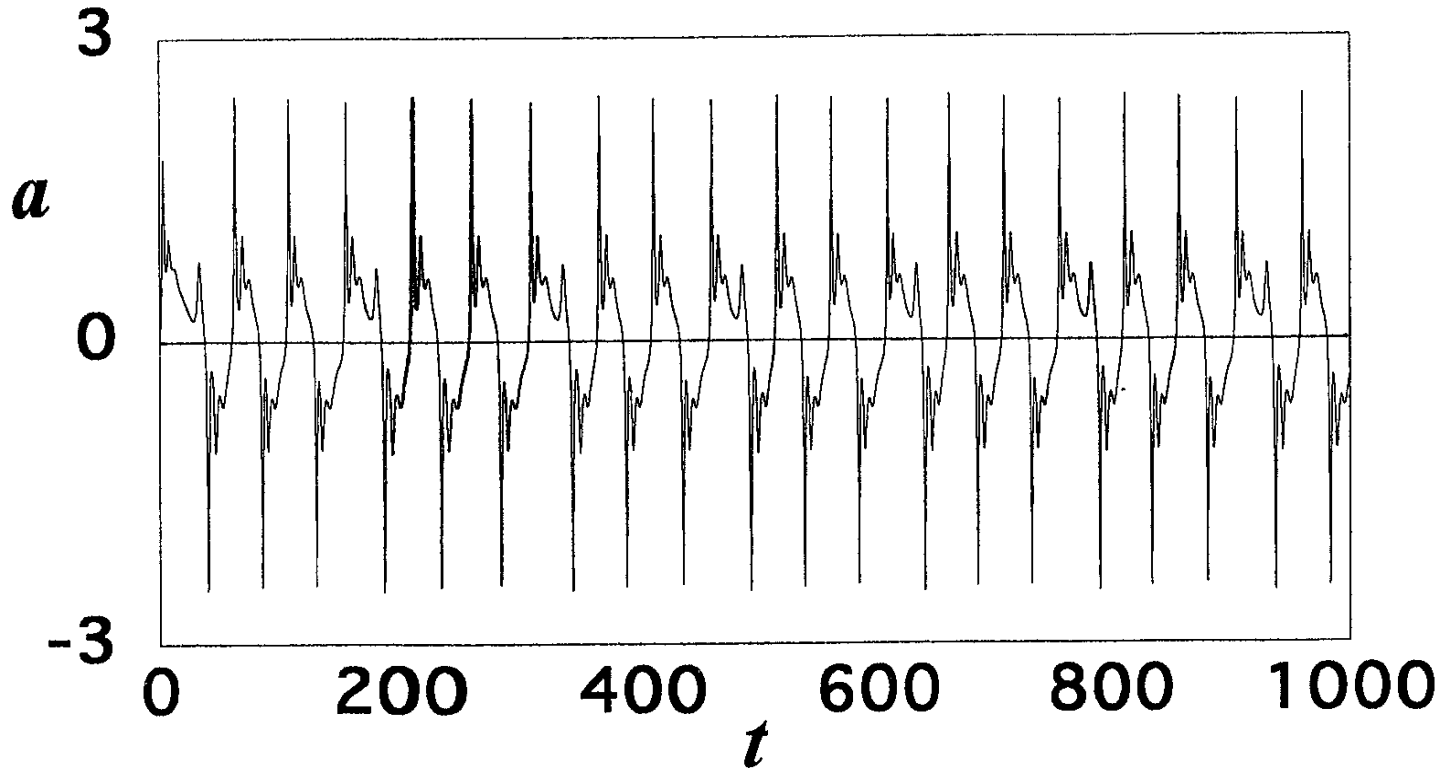

Fig . 18(b)

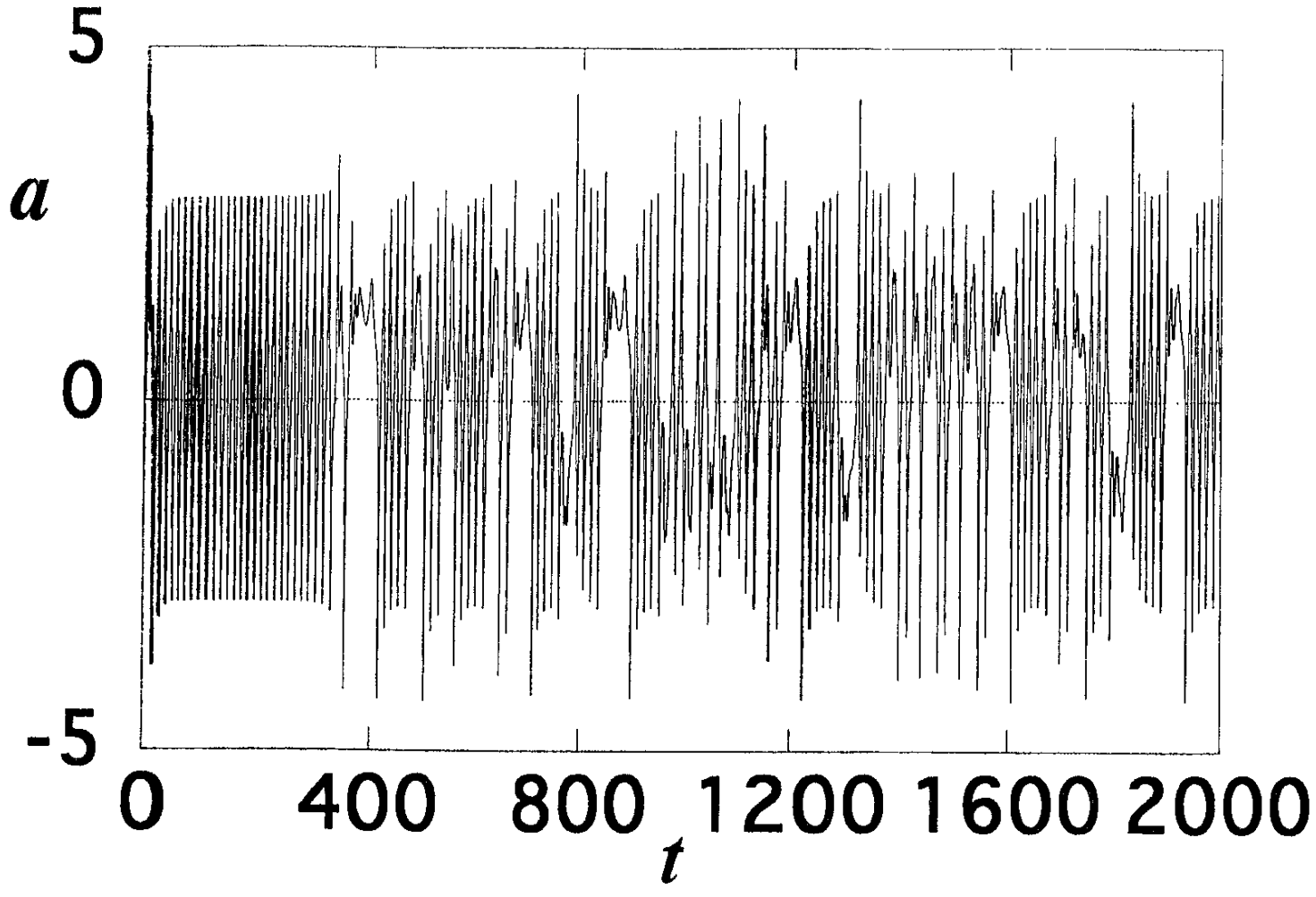

Fig . 19(a)

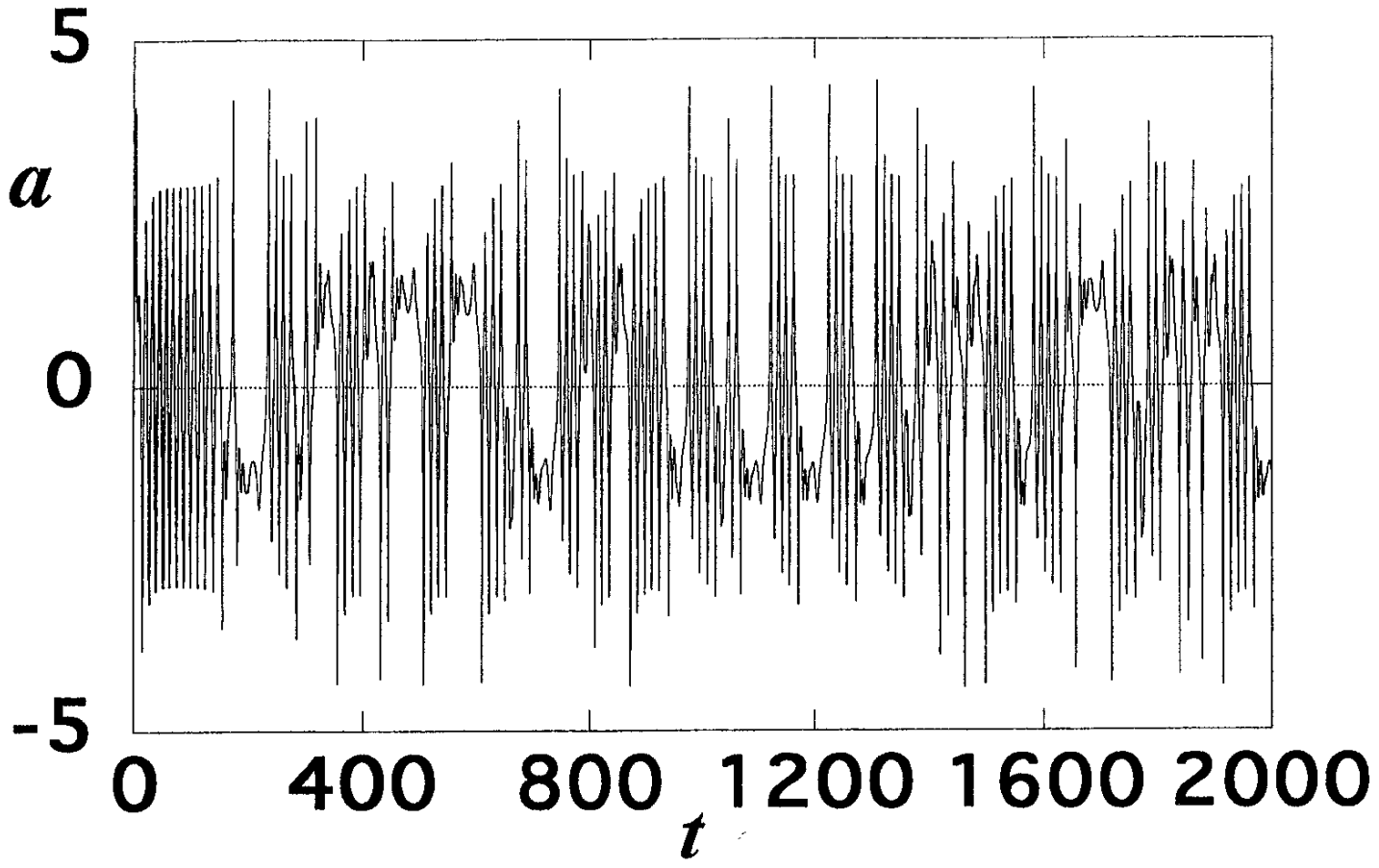

Fig . 19(b)

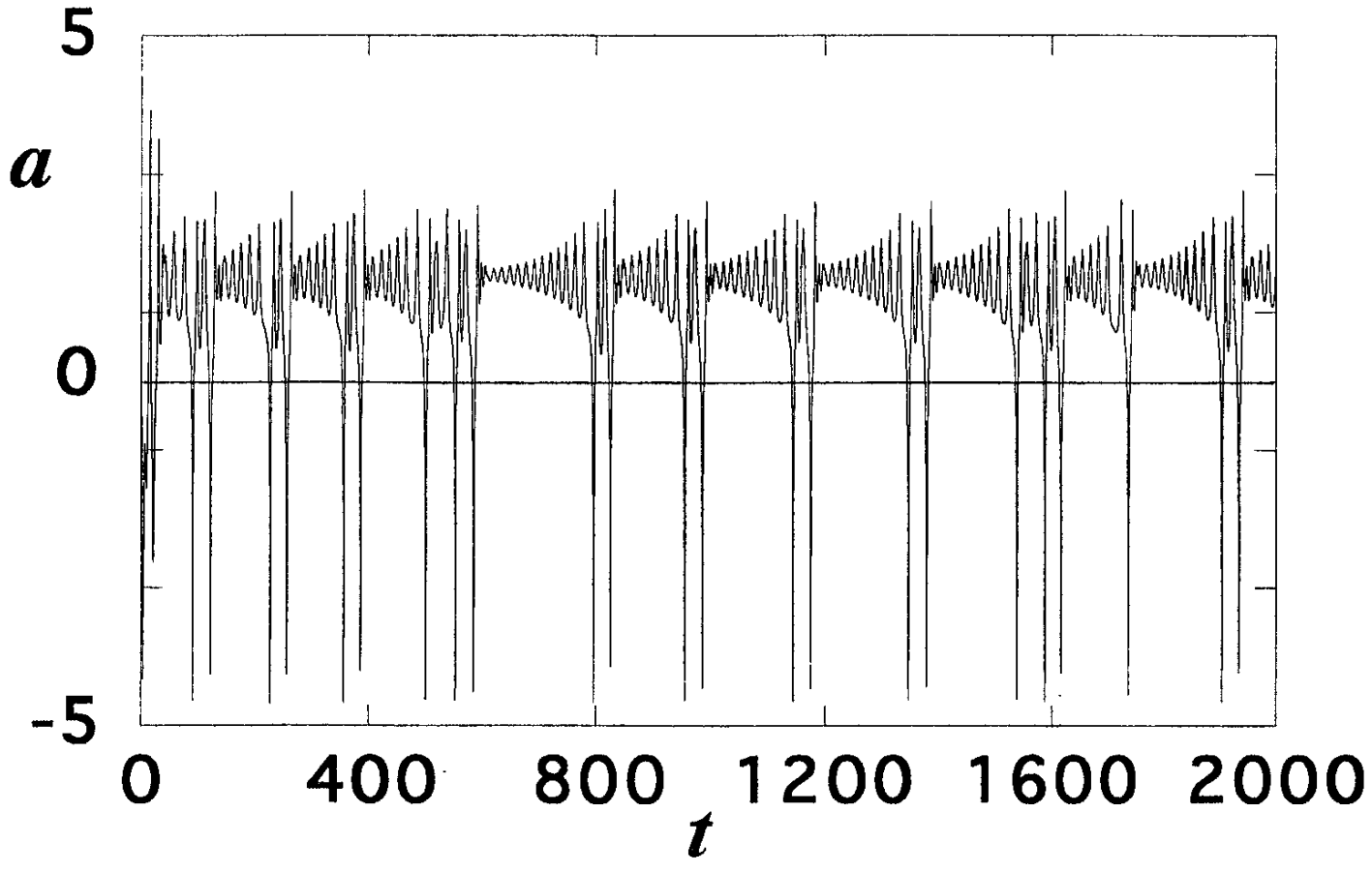

Fig . 19(c)

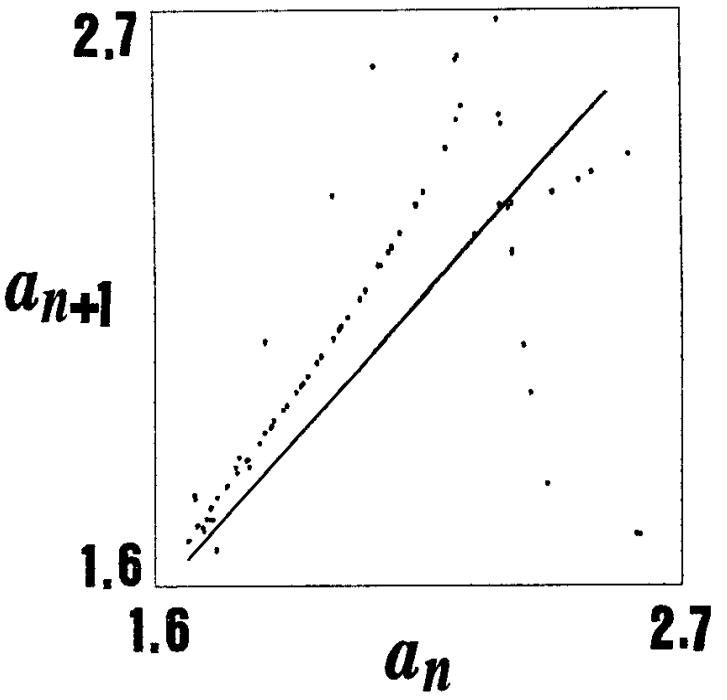

Fig . 20

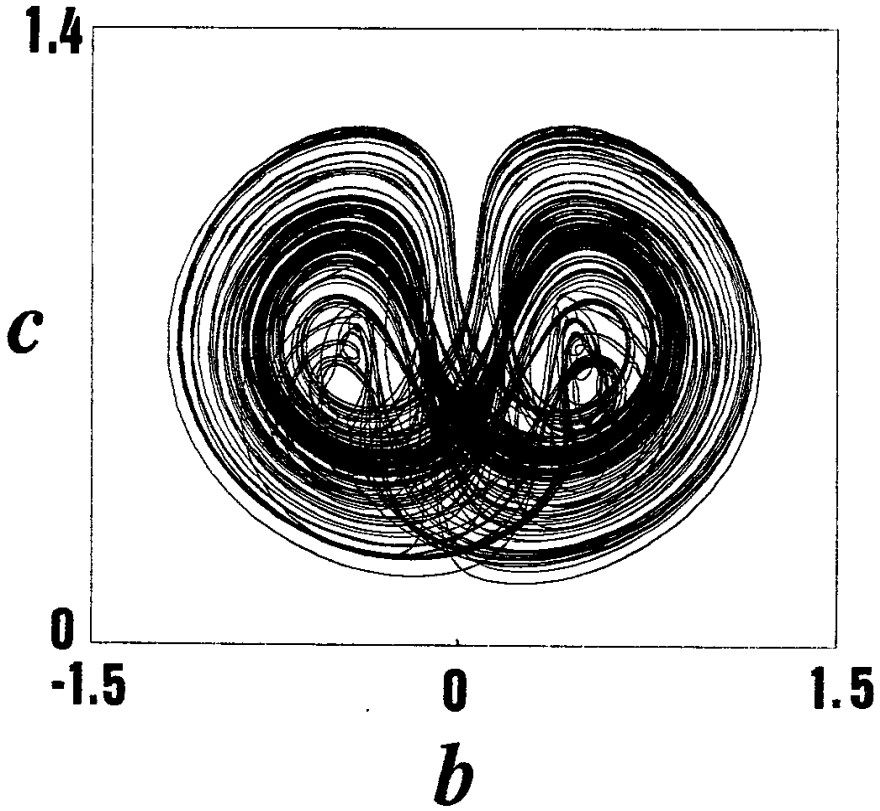

Fig . 21

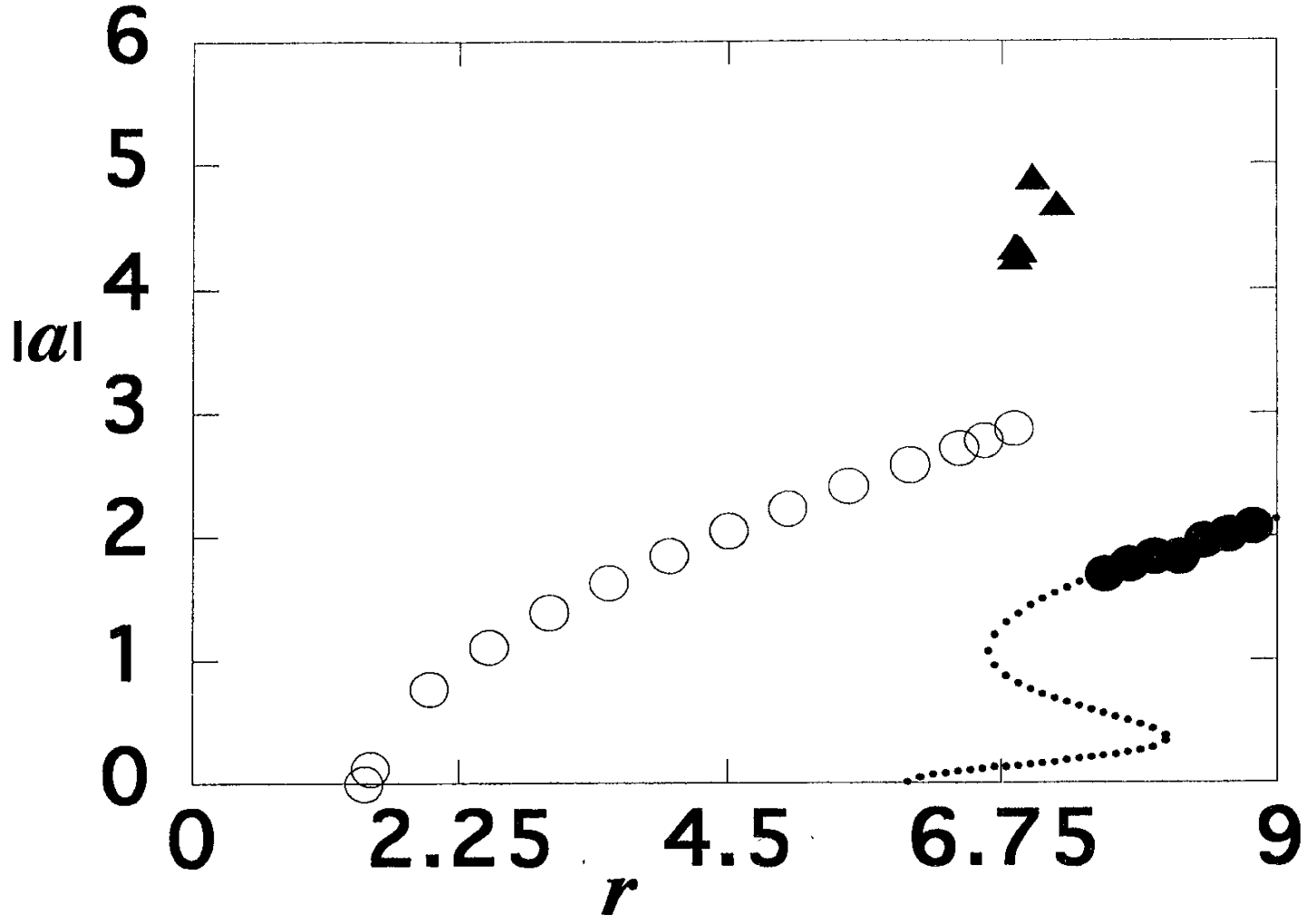

Fig . 22

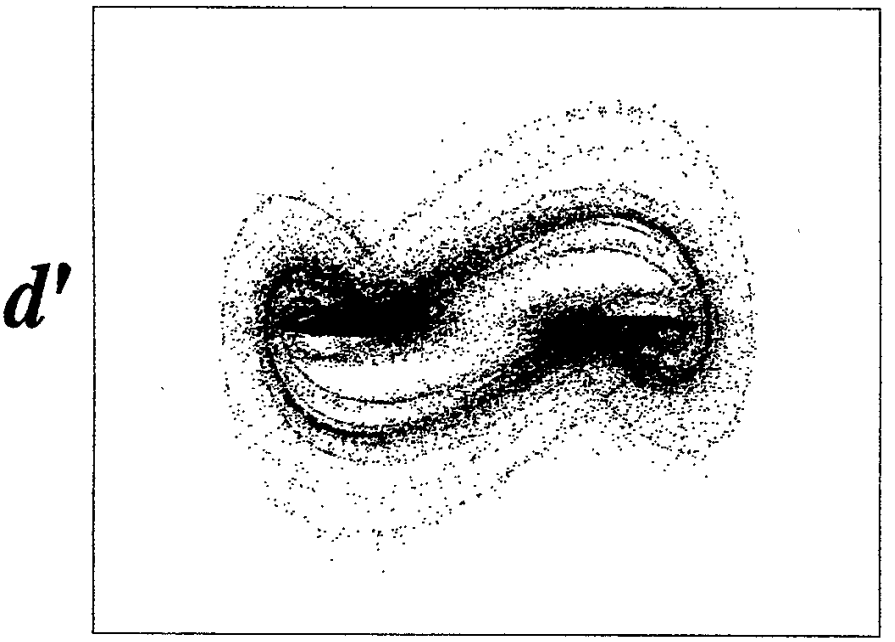

Fig . 23

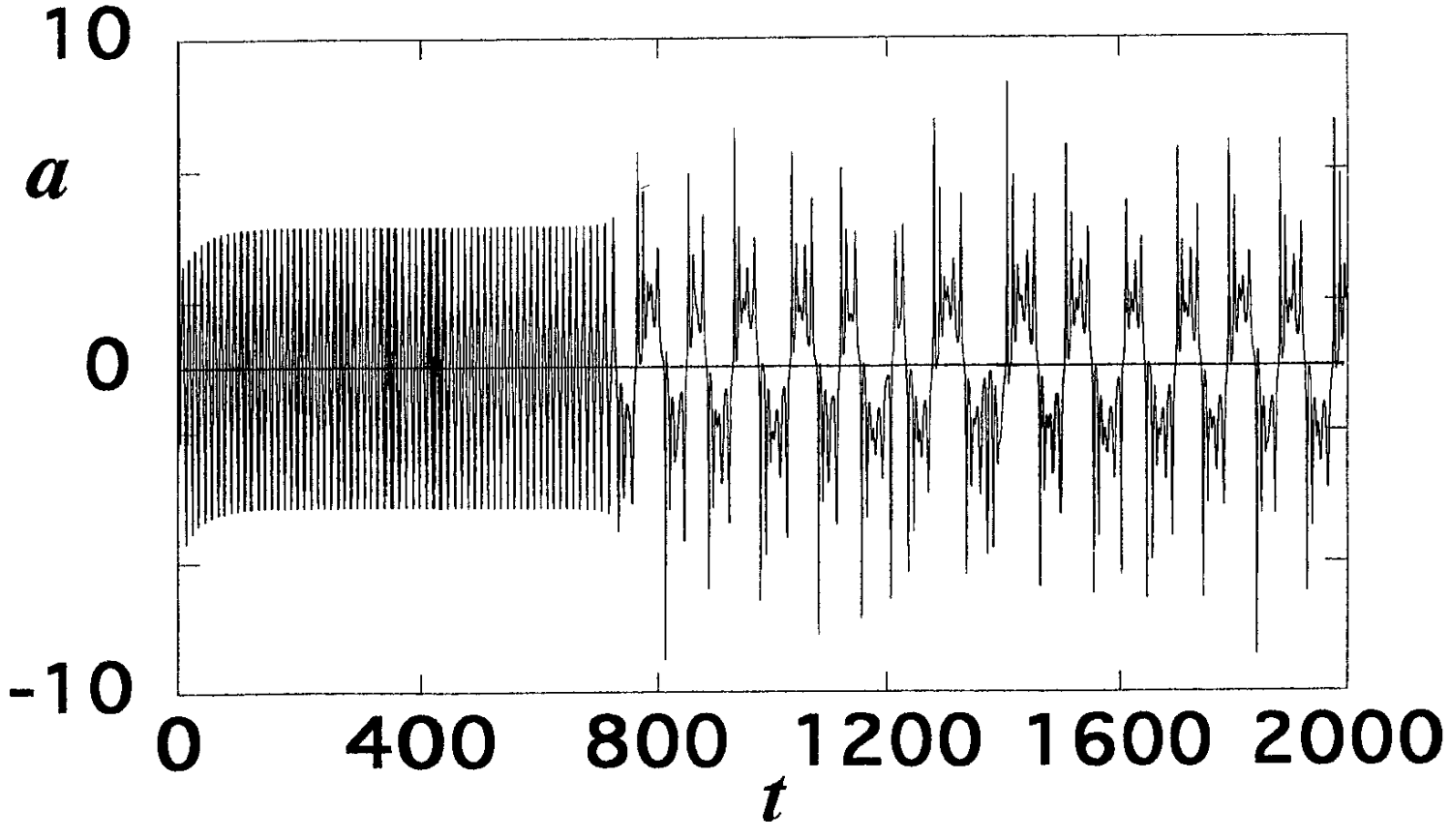

Fig . 24

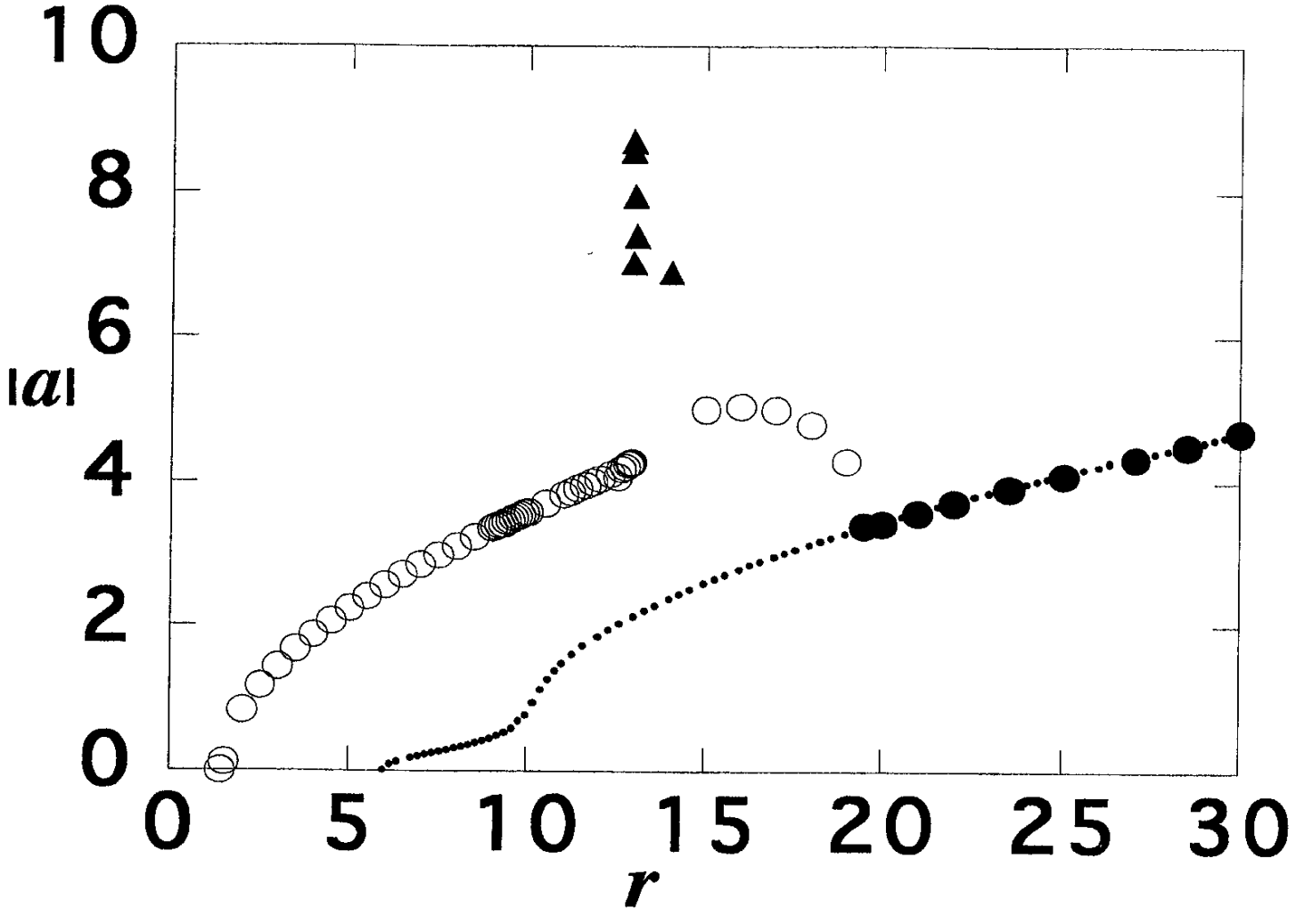

Fig . 25

Recent Issues of NIFS Series

NIFS-292 N. Noda, A. Sagara, H. Yamada, Y. Kubota, N. Inoue, K. Akaishi, O. Motojima, K. Iwamoto, M. Hashiba, I. Fujita, T. Hino, T. Yamashina, K. Okazaki, J. Rice, M. Yamage, H. Toyoda and H. Sugai,
Boronization Study for Application to Large Helical Device; July 1994

NIFS-293 Y. Ueda, T. Tanabe, V. Philipps, L. Könen, A. Pospieszczyk, U. Samm, B. Schweer, B. Unterberg, M. Wada, N. Hawkes and N. Noda,
Effects of Impurities Released from High Z Test Limiter on Plasma Performance in TEXTOR; July. 1994

NIFS-294 K. Akaishi, Y. Kubota, K. Ezaki and O. Motojima,
Experimental Study on Scaling Law of Outgassing Rate with A Pumping Parameter, Aug. 1994

NIFS-295 S. Bazdenkov, T. Sato, R. Horiuchi, K. Watanabe,
Magnetic Mirror Effect as a Trigger of Collisionless Magnetic Reconnection, Aug. 1994

NIFS-296 K. Itoh, M. Yagi, S.-I. Itoh, A. Fukuyama, H. Sanuki, M. Azumi,
Anomalous Transport Theory for Toroidal Helical Plasmas,
Aug. 1994 (IAEA-CN-60/D-III-3)

NIFS-297 J. Yamamoto, O. Motojima, T. Mito, K. Takahata, N. Yanagi, S. Yamada, H. Chikaraishi, S. Imagawa, A. Iwamoto, H. Kaneko, A. Nishimura, S. Satoh, T. Satow, H. Tamura, S. Yamaguchi, K. Yamazaki, M. Fujiwara, A. Iiyoshi and LHD group,
New Evaluation Method of Superconductor Characteristics for Realizing the Large Helical Device; Aug. 1994 (IAEA-CN-60/F-P-3)

NIFS-298 A. Komori, N. Ohyabu, T. Watanabe, H. Suzuki, A. Sagara, N. Noda, K. Akaishi, N. Inoue, Y. Kubota, O Motojima, M. Fujiwara and A. Iiyoshi,
Local Island Divertor Concept for LHD; Aug. 1994 (IAEA-CN-60/F-P-4)

NIFS-299 K. Toi, T. Morisaki, S. Sakakibara, A. Ejiri, H. Yamada, S. Morita, K. Tanaka, N. Nakajima, S. Okamura, H. Iguchi, K. Ida, K. Tsumori, S. Ohdachi, K. Nishimura, K. Matsuoka, J. Xu, I. Yamada, T. Minami, K. Narihara, R. Akiyama, A. Ando, H. Arimoto, A. Fujisawa, M. Fujiwara, H. Idei, O. Kaneko, K. Kawahata, A. Komori, S. Kubo, R. Kumazawa, T. Ozaki, A. Sagara, C. Takahashi, Y. Takita and T. Watari,
Impact of Rotational-Transform Profile Control on Plasma Confinement and Stability in CHS; Aug. 1994 (IAEA-CN-60/A6/C-P-3)

NIFS-300 H. Sugama and W. Horton,
Dynamical Model of Pressure-Gradient-Driven Turbulence and Shear Flow Generation in L-H Transition; Aug. 1994 (IAEA/CN-60/D-P-I-11)

NIFS-301 Y. Hamada, A. Nishizawa, Y. Kawasumi, K.N. Sato, H. Sakakita, R. Liang, K. Kawahata, A. Ejiri, K. Narihara, K. Sato, T. Seki, K. Toi, K. Itoh, H. Iguchi, A. Fujisawa, K. Adachi, S. Hidekuma, S. Hirokura, K. Ida, M. Kojima, J. Koog, R. Kumazawa, H. Kuramoto, T. Minami, I. Negi, S. Ohdachi, M. Sasao, T. Tsuzuki, J. Xu, I. Yamada, T. Watari, *Study of Turbulence and Plasma Potential in JIPP T-IIU Tokamak*; Aug. 1994 (IAEA/CN-60/A-2-III-5)

NIFS-302 K. Nishimura, R. Kumazawa, T. Mutoh, T. Watari, T. Seki, A. Ando, S. Masuda, F. Shinpo, S. Murakami, S. Okamura, H. Yamada, K. Matsuoka, S. Morita, T. Ozaki, K. Ida, H. Iguchi, I. Yamada, A. Ejiri, H. Idei, S. Muto, K. Tanaka, J. Xu, R. Akiyama, H. Arimoto, M. Isobe, M. Iwase, O. Kaneko, S. Kubo, T. Kawamoto, A. Lazaros, T. Morisaki, S. Sakakibara, Y. Takita, C. Takahashi and K. Tsumori, *ICRF Heating in CHS*; Sep. 1994 (IAEA-CN-60/A-6-I-4)

NIFS-303 S. Okamura, K. Matsuoka, K. Nishimura, K. Tsumori, R. Akiyama, S. Sakakibara, H. Yamada, S. Morita, T. Morisaki, N. Nakajima, K. Tanaka, J. Xu, K. Ida, H. Iguchi, A. Lazaros, T. Ozaki, H. Arimoto, A. Ejiri, M. Fujiwara, H. Idei, A. Iiyoshi, O, Kaneko, K. Kawahata, T. Kawamoto, S. Kubo, T. Kuroda, O. Motojima, V.D. Pustovitov, A. Sagara, C. Takahashi, K. Toi and I. Yamada, *High Beta Experiments in CHS*; Sep. 1994 (IAEA-CN-60/A-2-IV-3)

NIFS-304 K. Ida, H. Idei, H. Sanuki, K. Itoh, J. Xu, S. Hidekuma, K. Kondo, A. Sahara, H. Zushi, S.-I. Itoh, A. Fukuyama, K. Adati, R. Akiyama, S. Bessho, A. Ejiri, A. Fujisawa, M. Fujiwara, Y. Hamada, S. Hirokura, H. Iguchi, O. Kaneko, K. Kawahata, Y. Kawasumi, M. Kojima, S. Kubo, H. Kuramoto, A. Lazaros, R. Liang, K. Matsuoka, T. Minami, T. Mizuuchi, T. Morisaki, S. Morita, K. Nagasaki, K. Narihara, K. Nishimura, A. Nishizawa, T. Obiki, H. Okada, S. Okamura, T. Ozaki, S. Sakakibara, H. Sakakita, A. Sagara, F. Sano, M. Sasao, K. Sato, K.N. Sato, T. Saeki, S. Sudo, C. Takahashi, K. Tanaka, K. Tsumori, H.Yamada, I. Yamada, Y. Takita, T. Tuzuki, K. Toi and T. Watari, *Control of Radial Electric Field in Torus Plasma;* Sep. 1994 (IAEA-CN-60/A-2-IV-2)

NIFS-305 T. Hayashi, T. Sato, N. Nakajima, K. Ichiguchi, P. Merkel, J. Nührenberg, U. Schwenn, H. Gardner, A. Bhattacharjee and C.C.Hegna, *Behavior of Magnetic Islands in 3D MHD Equilibria of Helical Devices*; Sep. 1994 (IAEA-CN-60/D-2-II-4)

NIFS-306 S. Murakami, M. Okamoto, N. Nakajima, K.Y. Watanabe, T. Watari, T. Mutoh, R. Kumazawa and T. Seki, *Monte Carlo Simulation for ICRF Heating in Heliotron/Torsatrons*; Sep. 1994 (IAEA-CN-60/D-P-I-14)

NIFS-307 Y. Takeiri, A. Ando, O. Kaneko, Y. Oka, K. Tsumori, R. Akiyama, E. Asano,

T. Kawamoto, T. Kuroda, M. Tanaka and H. Kawakami,
Development of an Intense Negative Hydrogen Ion Source with a Wide-Range of External Magnetic Filter Field; Sep. 1994

NIFS-308 T. Hayashi, T. Sato, H.J. Gardner and J.D. Meiss,
Evolution of Magnetic Islands in a Heliac; Sep. 1994

NIFS-309 H. Amo, T. Sato and A. Kageyama,
Intermittent Energy Bursts and Recurrent Topological Change of a Twisting Magnetic Flux Tube; Sep.1994

NIFS-310 T. Yamagishi and H. Sanuki,
Effect of Anomalous Plasma Transport on Radial Electric Field in Torsatron/Heliotron; Sep. 1994

NIFS-311 K. Watanabe, T. Sato and Y. Nakayama,
Current-profile Flattening and Hot Core Shift due to the Nonlinear Development of Resistive Kink Mode; Oct. 1994

NIFS-312 M. Salimullah, B. Dasgupta, K. Watanabe and T. Sato,
Modification and Damping of Alfvén Waves in a Magnetized Dusty Plasma; Oct. 1994

NIFS-313 K. Ida, Y. Miura, S -I. Itoh, J.V. Hofmann, A. Fukuyama, S. Hidekuma, H. Sanuki, H. Idei, H. Yamada, H. Iguchi, K. Itoh,
Physical Mechanism Determining the Radial Electric Field and its Radial Structure in a Toroidal Plasma; Oct. 1994

NIFS-314 Shao-ping Zhu, R. Horiuchi, T. Sato and The Complexity Simulation Group,
Non-Taylor Magnetohydrodynamic Self-Organization; Oct. 1994

NIFS-315 M. Tanaka,
Collisionless Magnetic Reconnection Associated with Coalescence of Flux Bundles; Nov. 1994

NIFS-316 M. Tanaka,
Macro-EM Particle Simulation Method and A Study of Collisionless Magnetic Reconnection; Nov. 1994

NIFS-317 A. Fujisawa, H. Iguchi, M. Sasao and Y. Hamada,
Second Order Focusing Property of 210° Cylindrical Energy Analyzer; Nov. 1994

NIFS-318 T. Sato and Complexity Simulation Group,
Complexity in Plasma - A Grand View of Self- Organization; Nov. 1994

NIFS-319 Y. Todo, T. Sato, K. Watanabe, T.H. Watanabe and R. Horiuchi,
MHD-Vlasov Simulation of the Toroidal Alfvén Eigenmode; Nov. 1994

NIFS-320 A. Kageyama, T. Sato and The Complexity Simulation Group,

Computer Simulation of a Magnetohydrodynamic Dynamo II: Nov. 1994

NIFS-321 A. Bhattacharjee, T. Hayashi, C.C.Hegna, N. Nakajima and T. Sato, *Theory of Pressure-induced Islands and Self-healing in Three-dimensional Toroidal Magnetohydrodynamic Equilibria;* Nov. 1994

NIFS-322 A. Iiyoshi, K. Yamazaki and the LHD Group, *Recent Studies of the Large Helical Device;* Nov. 1994

NIFS-323 A. Iiyoshi and K. Yamazaki, *The Next Large Helical Devices*; Nov. 1994

NIFS-324 V.D. Pustovitov *Quasisymmetry Equations for Conventional Stellarators*; Nov. 1994

NIFS-325 A. Taniike, M. Sasao, Y. Hamada, J. Fujita, M. Wada, *The Energy Broadening Resulting from Electron Stripping Process of a Low Energy Au^- Beam;* Dec. 1994

NIFS-326 I. Viniar and S. Sudo, *New Pellet Production and Acceleration Technologies for High Speed Pellet Injection System "HIPEL" in Large Helical Device;* Dec. 1994

NIFS-327 Y. Hamada, A. Nishizawa, Y. Kawasumi, K. Kawahata, K. Itoh, A. Ejiri, K. Toi, K. Narihara, K. Sato, T. Seki, H. Iguchi, A. Fujisawa, K. Adachi, S. Hidekuma, S. Hirokura, K. Ida, M. Kojima, J. Koong, R. Kumazawa, H. Kuramoto, R. Liang, T. Minami, H. Sakakita, M. Sasao, K.N. Sato, T. Tsuzuki, J. Xu, I. Yamada, T. Watari, *Fast Potential Change in Sawteeth in JIPP T-IIU Tokamak Plasmas*; Dec. 1994

NIFS-328 V.D. Pustovitov, *Effect of Satellite Helical Harmonics on the Stellarator Configuration;* Dec. 1994

NIFS-329 K. Itoh, S-I. Itoh and A. Fukuyama, *A Model of Sawtooth Based on the Transport Catastrophe*; Dec. 1994

NIFS-330 K. Nagasaki, A. Ejiri, *Launching Conditions for Electron Cyclotron Heating in a Sheared Magnetic Field*; Jan. 1995

NIFS-331 T.H. Watanabe, Y. Todo, R. Horiuchi, K. Watanabe, T. Sato, *An Advanced Electrostatic Particle Simulation Algorithm for Implicit Time Integration;* Jan. 1995